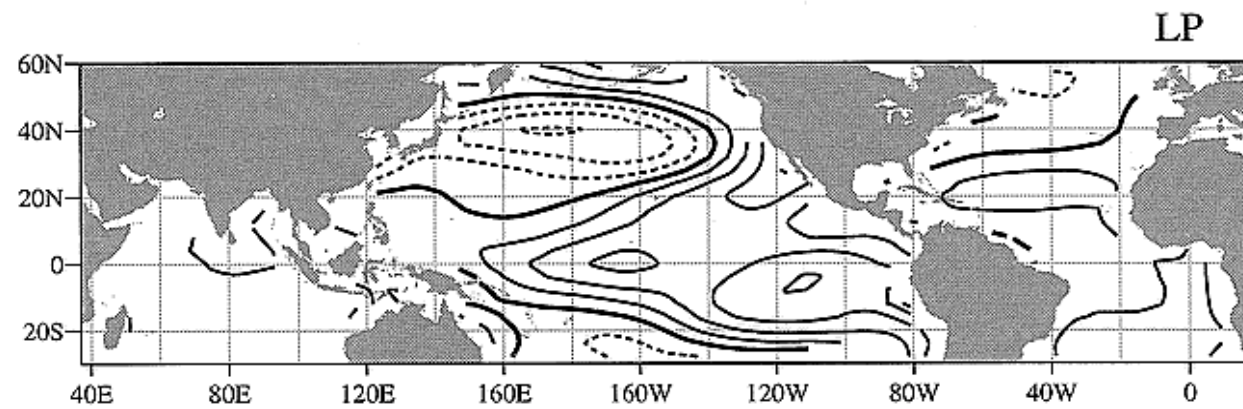
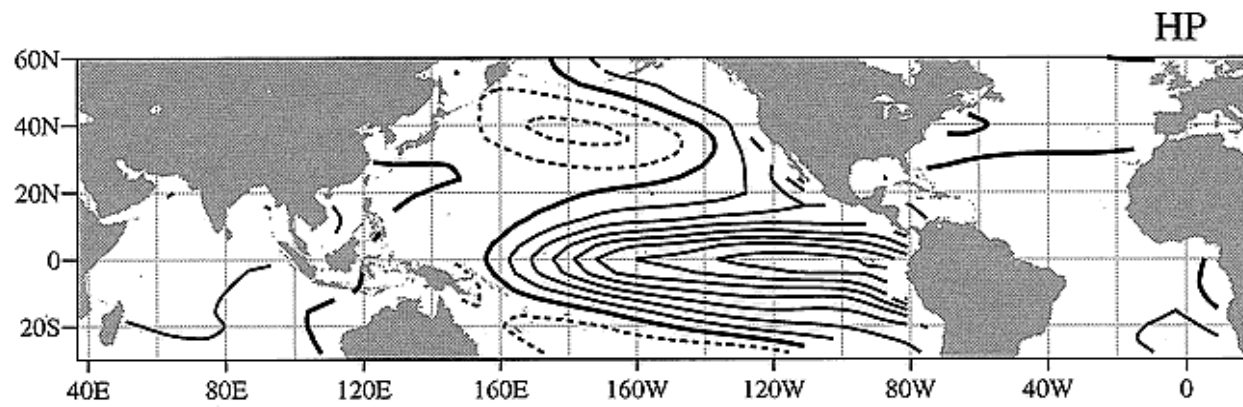
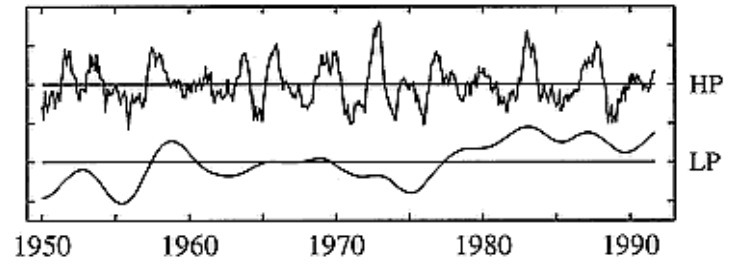


Extratropical Air-Sea Interaction – Decadal Variability

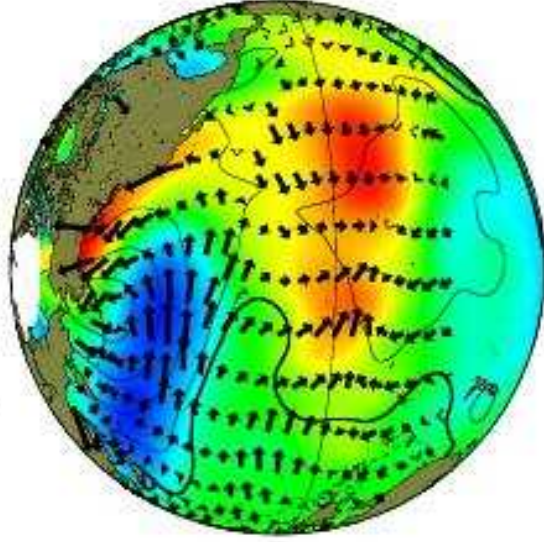
1. Observations in the North Pacific
2. Role of stochastic forcing
 - Red spectrum
 - Basic effect of air-sea thermal feedback
 - Reemergence
 - Nonlocal response to stochastic forcing
3. Extratropical ocean to atmosphere feedback
4. Mechanism of decadal variability



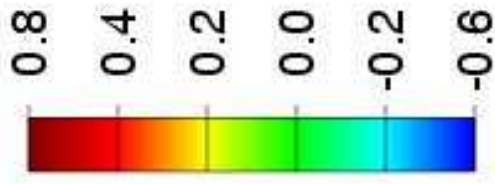
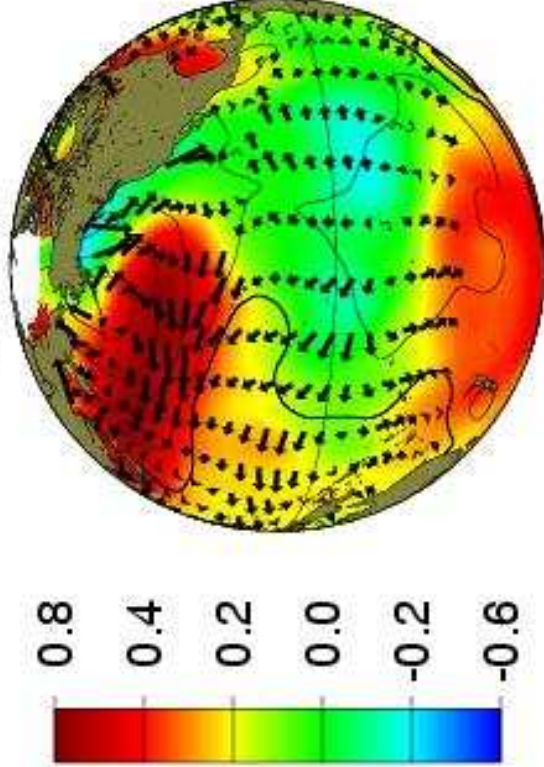
Zhang, Wallace, Battisti 1997

Pacific Decadal Oscillation

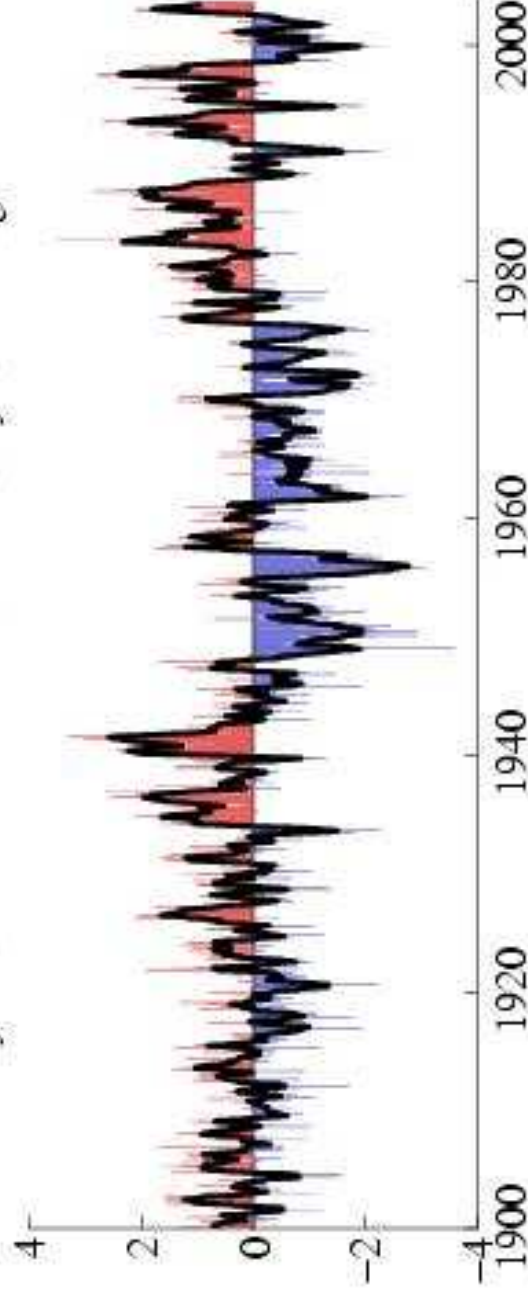
positive phase



negative phase



monthly values for the PDO index: January 1900–August 2003



FIGURES

Pacific Decadal Oscillation

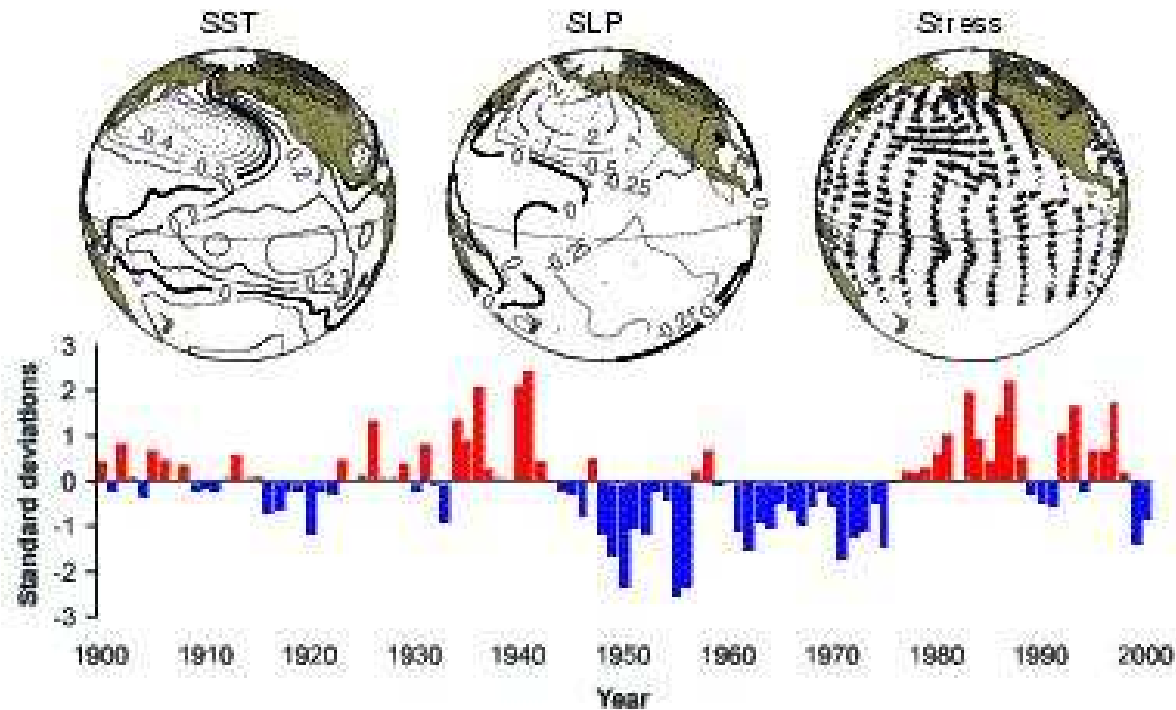
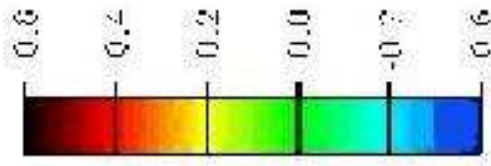
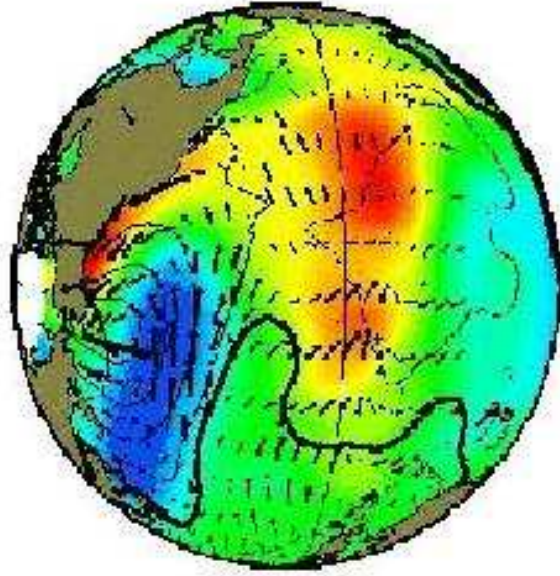
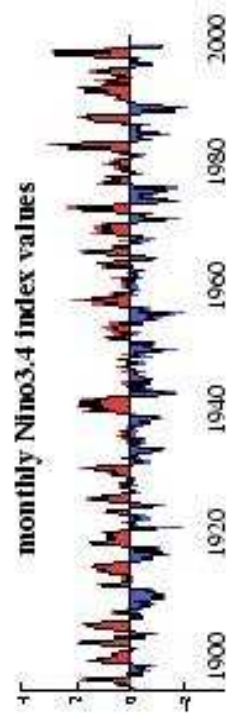
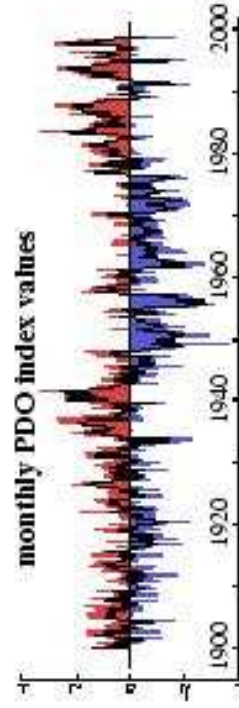
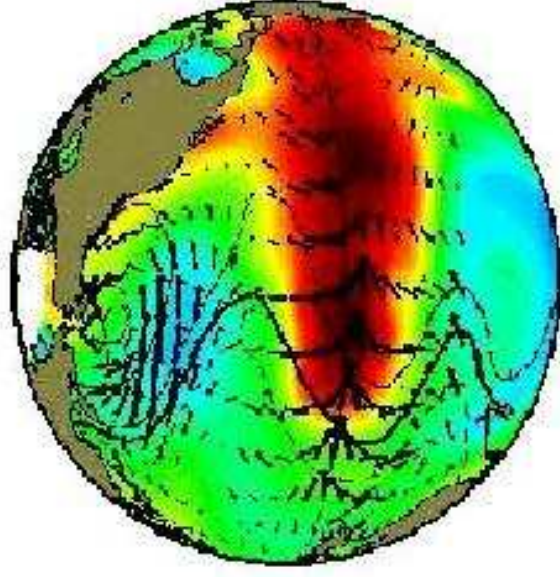


FIGURE 1: (top) Anomalous climate conditions associated with the warm phases of the Pacific Decadal Oscillation (PDO), and (bottom) November-March average values of the PDO index. Values shown are $^{\circ}\text{C}$ for sea surface temperature (SST), millibars for sea level pressure (SLP) and direction and intensity of surface wind stress. The longest wind vectors represent a pseudostress of $10 \text{ m}^2/\text{s}^2$. Actual anomaly values for a given year at a given location are obtained by multiplying the climate anomaly by the associated index value. Adapted and updated from Mantua et al. (1997)

Pacific Decadal Oscillation



El Niño/Southern Oscillation



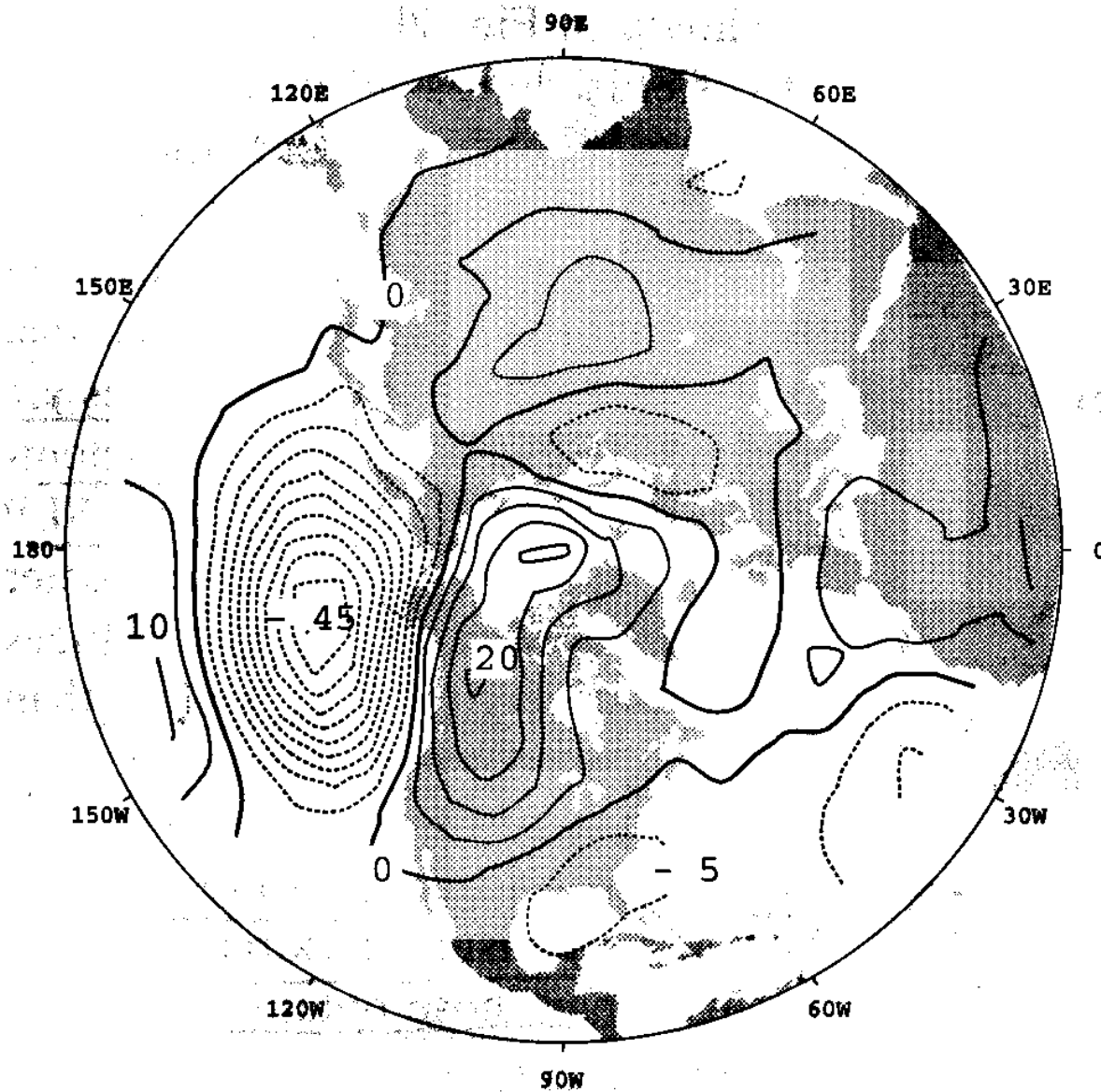
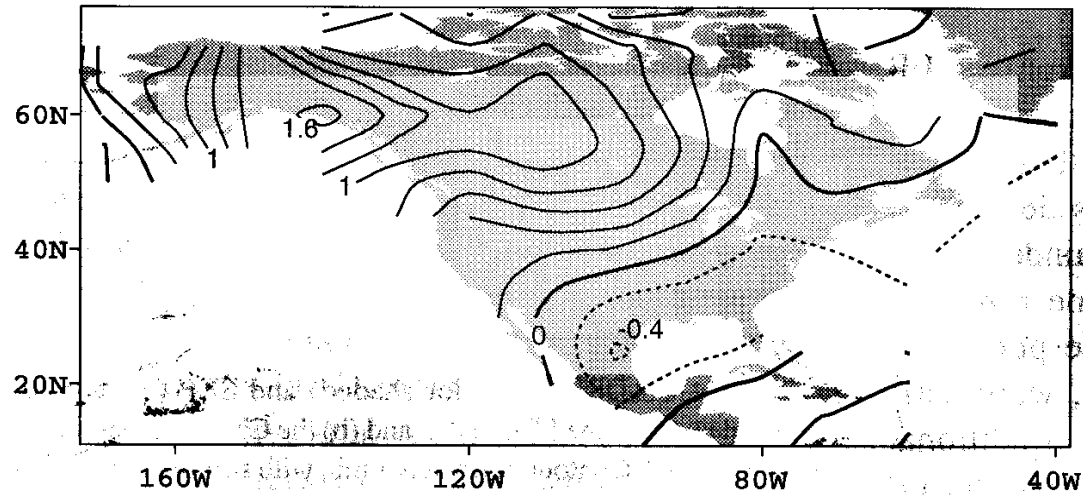


FIG. 4. Wintertime Northern Hemisphere 500-mb heights regressed upon the PDO index for the period of record 1951–90. Contour interval is 5 m, positive (negative) contours are solid (dashed).

(a) Nov–Mar surface air temperature regressed on the PDO index ($^{\circ}\text{C}$): 1900–1992



(b) Dec–Feb precipitation correlations with the PDO index ($\times 100$): 1900–1992

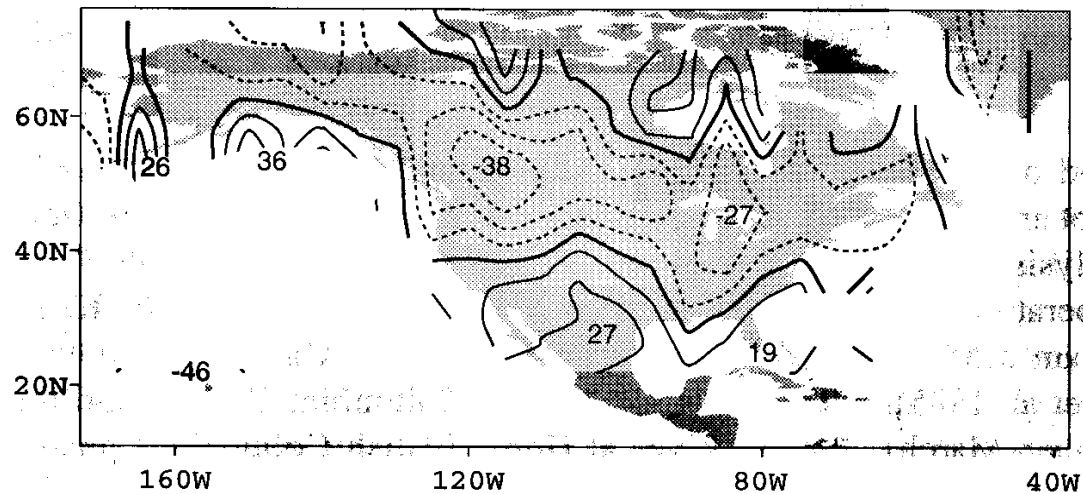


FIG. 3. Maps of PDO regression and correlation coefficients: (a) November–March surface air temperature regressed upon the PDO index shown in Fig. 1; contour interval is 0.2°C . (b) Correlation coefficients ($\times 100$) between December–February precipitation and the PDO index shown in Fig. 1; contour interval is 10. Positive (negative) contours are solid (dashed).

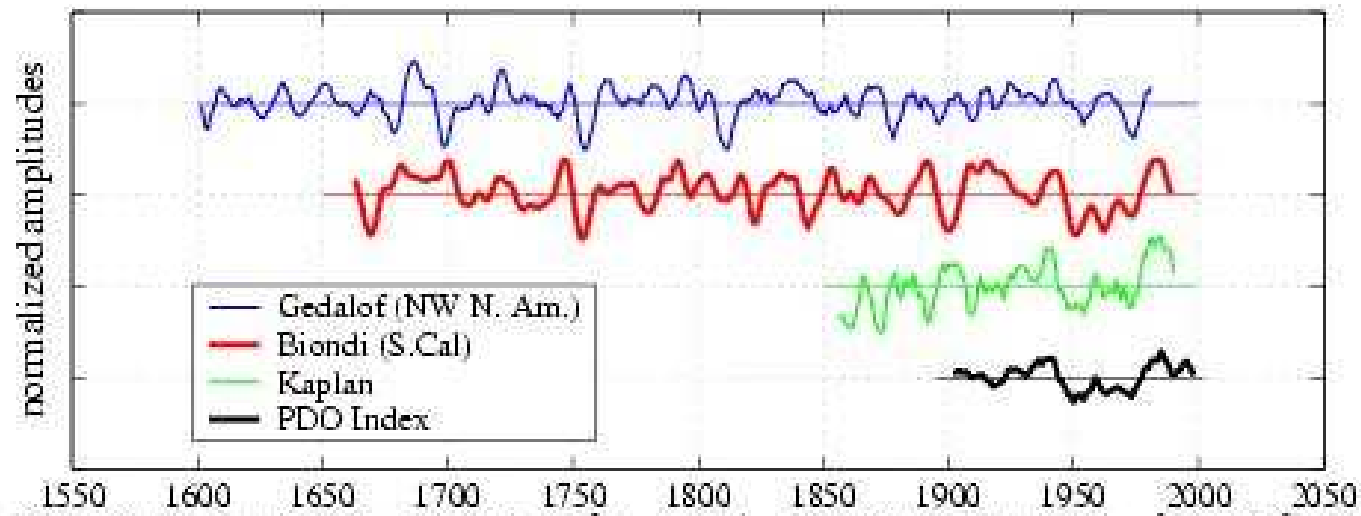


Figure 2: 5-year running average plots of tree-ring based PDO reconstructions of Gedalof and Smith (2001) and Biondi et al (2001), along with Kaplan et al.'s (2000) COADS SST index for 1854-1992 and Mantua et al.'s (1997) SST-based PDO index. Each time series has been normalized with respect to the available period of record, and they are plotted with an offset for clarity.

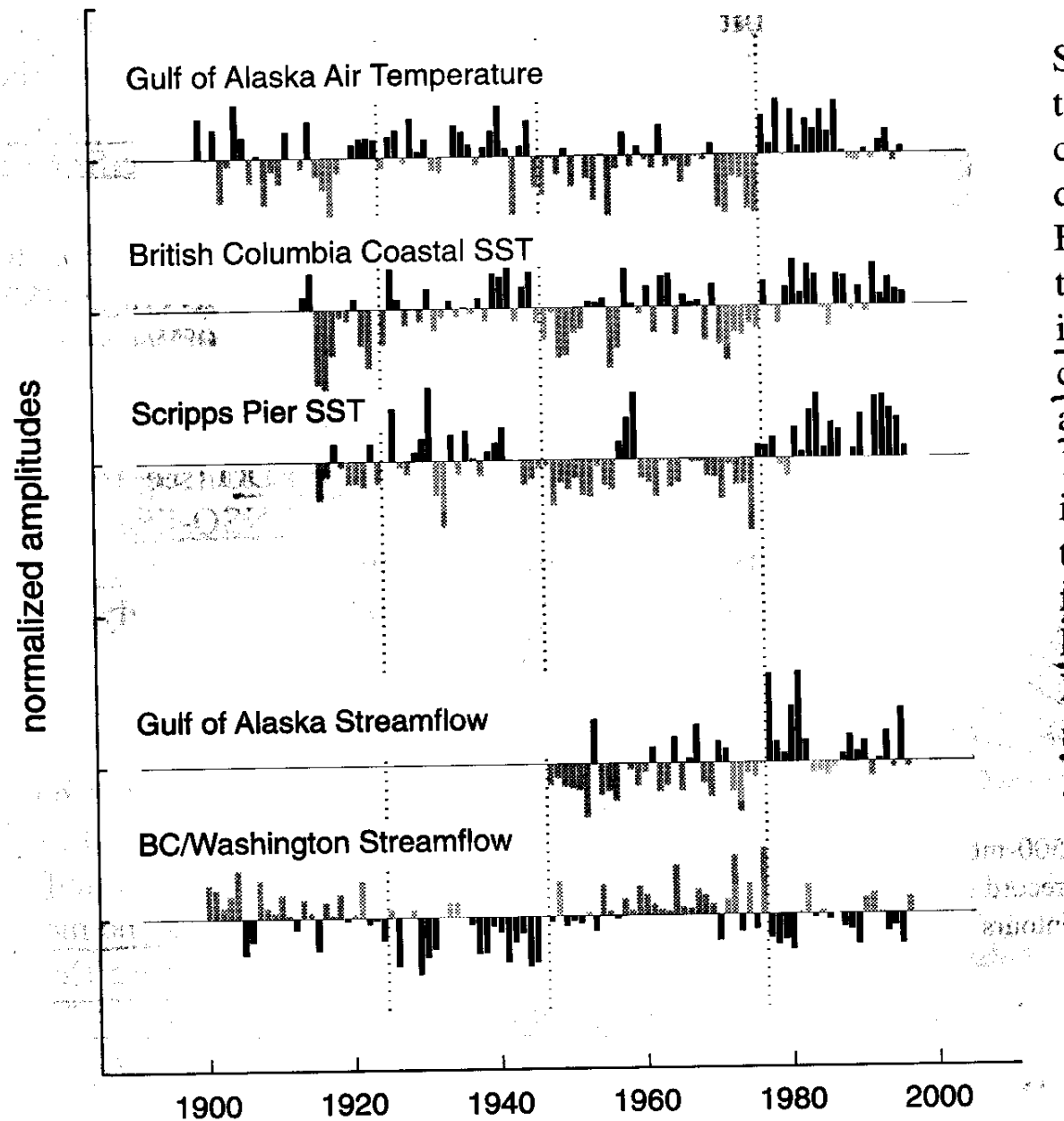


FIG. 5. Selected regional climate time series with PDO signatures. Dotted vertical lines are drawn to mark the PDO polarity reversal times in 1925, 1947, and 1977. Bars are shaded as in Fig. 1, with the shading convention reversed for the BC/Washington streamflow index.

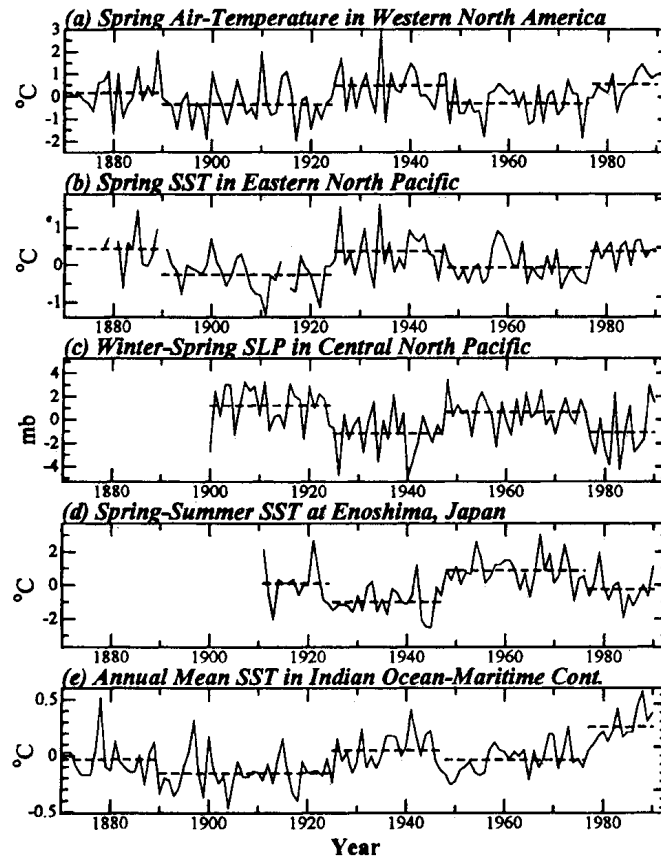


Figure 1. Time series of anomalies exhibiting coherent interdecadal climate changes (thin solid curve), with temporal averages of the anomalies for the periods 1870–1889, 1890–1924, 1925–1947, 1948–1976 and 1977–1990 (thick dashed lines). (a) Spring (Mar.–May) air-temperature anomalies in western North America averaged over 130°W–105°W, 30°N–55°N. The air-temperature anomaly is calculated relative to 1930–50 at each station, and then the anomalies are averaged spatially. (b) Spring SST anomalies in the eastern North Pacific averaged over 140°W–110°W, 30°N–55°N. The average is calculated when available grid points are more than 20% of total grid points in the spring of respective years. (c) Winter-spring (Dec.–May) SLP anomalies in the central North Pacific averaged over 160°E–140°W, 30°N–65°N. (d) Spring-summer (Mar.–Aug.) SST anomalies at Enoshima, Japan. (e) Annual mean SST anomalies in the Indian Ocean–maritime continent region averaged over 40°E–160°E, 15°S–15°N. All differences in the temporal average between successive periods are significant at the 95% confidence level in each time series.

Spring Air-Temp.

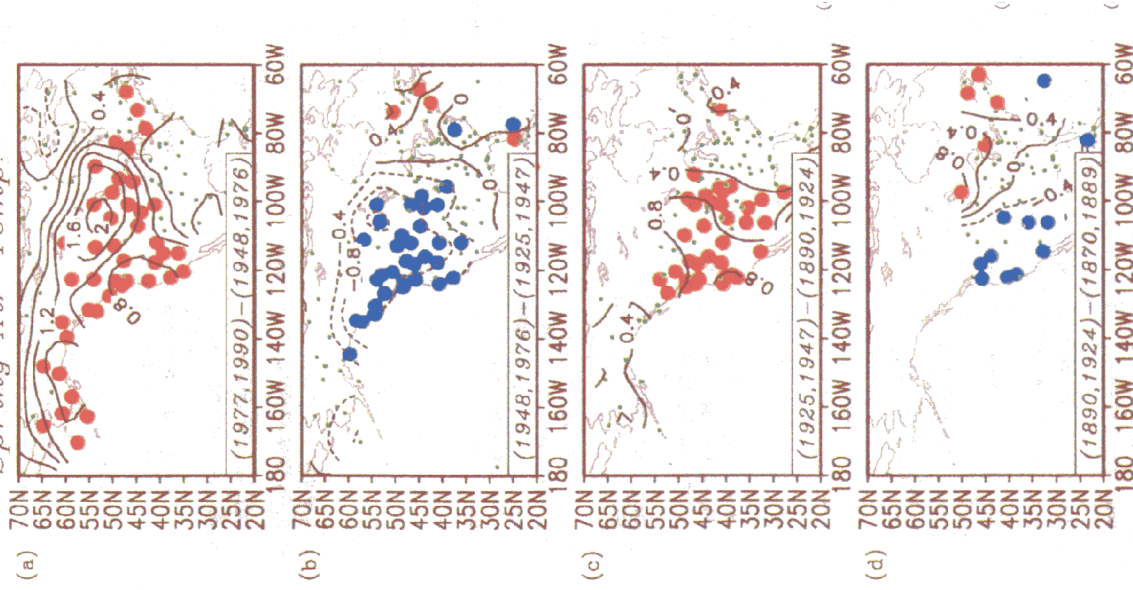
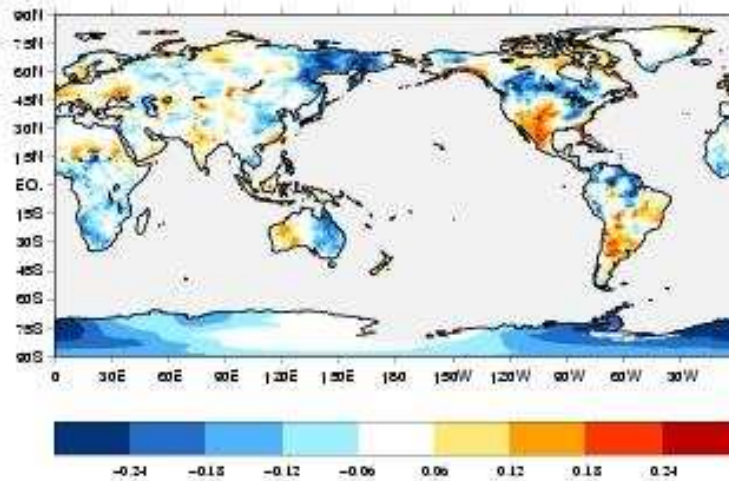


Figure 2. Spring air-temperature differences at the long-term weather stations between two periods: (a) 1977–1990 minus 1948–1976; (b) 1948–1976 minus 1925–1947; (c) 1925–1947 minus 1890–1924; and (d) 1890–1924 minus 1870–1889. A red (blue) closed circle indicates that the temperature increase (decrease) at the station is significant at the 95% confidence level, whereas a green dot indicates an insignificant difference. The contours indicate the amplitude of temperature differences, as calculated for respective stations and smoothed with a Gaussian filter of an e -folding length of 400 km. The contour interval is 0.4°C , and dashed contours indicate negative values.

0.5 Degree Grid November-April Precipitation
 correlated with November-April PDO index: 1950-96



0.5 Degree Grid November-April Temperature
 correlations with November-April PDO index: 1950-96

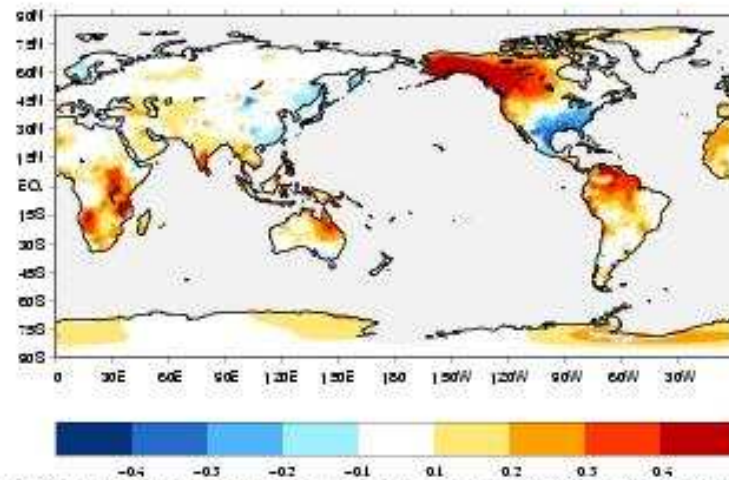


Figure 3: Correlations between November-April mean precipitation (top) and temperature (bottom) and the November-April mean PDO index. Precipitation and temperature data are the 0.5 Degree grid climatologically aided interpolation (CAI) fields produced at the University of Delaware by Coit Willmott and collaborators (available via the internet at <http://> (also see Willmott and Robeson 1995). Negative correlation coefficients are shaded in blues, positive correlation coefficients are shaded in reds and yellows.

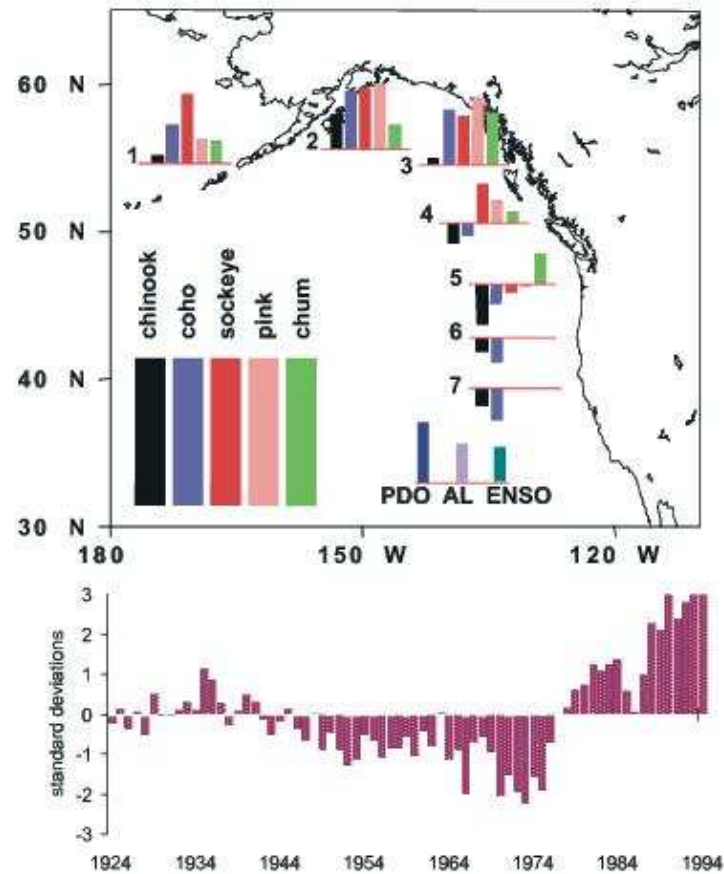


Figure 4. A graphical depiction of the "Inverse Production Regimes" of Hare et al. (1999). The bars represent loadings from a principal component analysis (PCA) of 30 salmon time series for the period 1925-1997. Regional definitions are as follows: 1 – Western Alaska, 2 – Central Alaska, 3 – Southeast Alaska, 4 – British Columbia, 5 – Washington, 6 – Oregon, 7 – California. Three climate indices were included in the PCA: Pacific Decadal Oscillation (PDO), Aleutian Low Pressure Index (AL) and the El Niño-Southern Oscillation (ENSO). The longest bar, Central Alaska pink salmon, represents a correlation coefficient with a value of 0.855, and represents the correlation between that time series and the illustrated temporal component (score) from the PCA.

PDO anomalies

Table 1 Summary of Pacific and North American climate anomalies associated with extreme phases of the PDO

Climate anomalies	Warm phase PDO	Cool phase PDO
Ocean surface temperatures in the northeastern and tropical Pacific	Above average	Below average
October – March northwestern North American air temperatures	Above average	Below average
October – March Southeastern US air temperatures	Below average	Above average
October – March southern US/Northern Mexico precipitation	Above average	Below average
October – March Northwestern North America and Great Lakes precipitation	Below average	Above average
Northwestern North American springtime snow pack and water year (October–September) stream flow	Below average	Above average

Modulates ENSO teleconnections
affects biology

Stochastic Forcing

$$\frac{dT}{dt} = -\lambda T + F$$

$$T(t) = \int_{t_0}^t dt' F(t') e^{-\lambda(t-t')} + e^{-\lambda(t-t_0)} T(t_0)$$

$$\tilde{T}(\omega)\tilde{T}^*(\omega) = \frac{\tilde{F}(\omega)\tilde{F}^*(\omega)}{\lambda^2 + \omega^2}$$

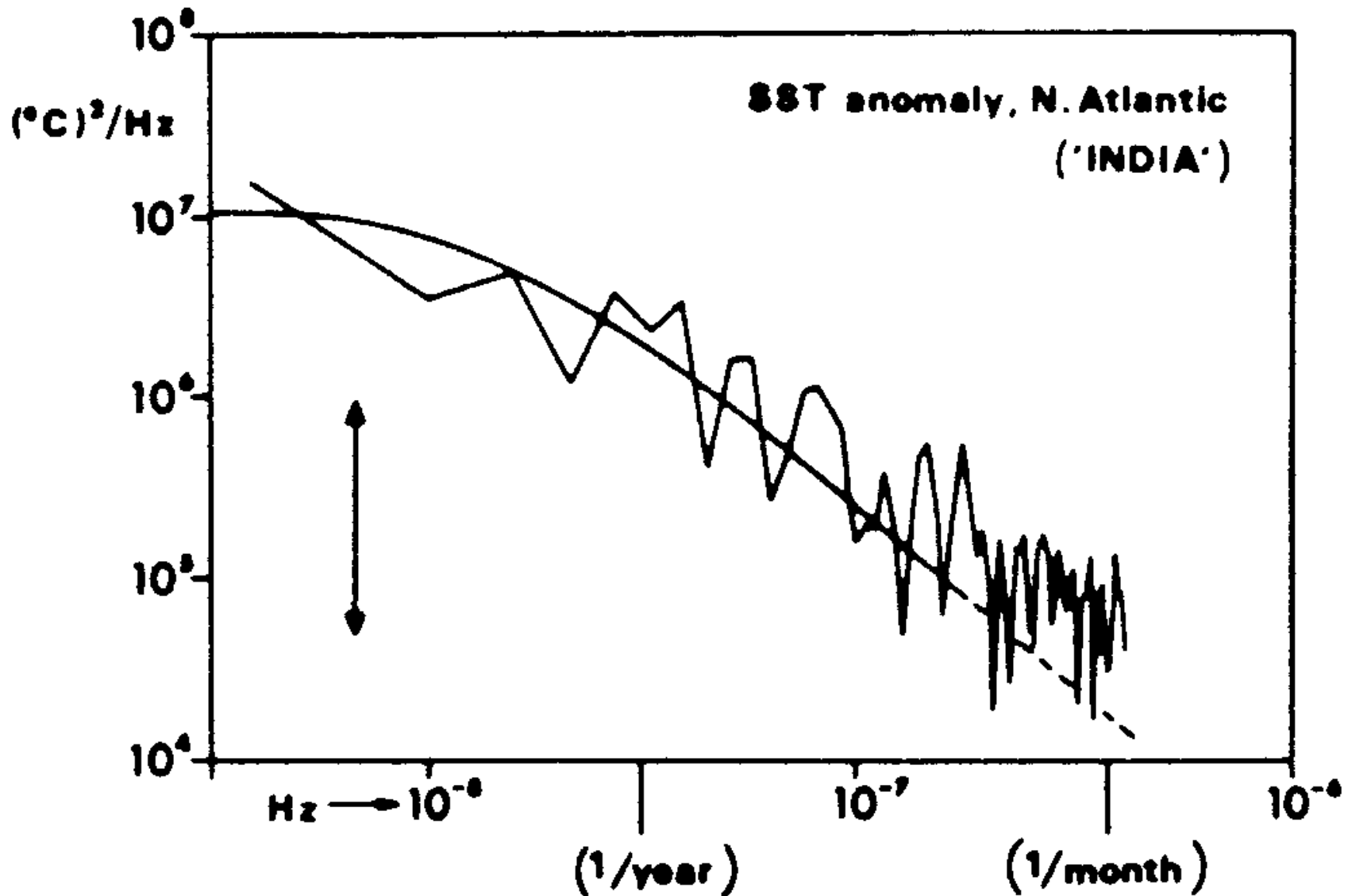
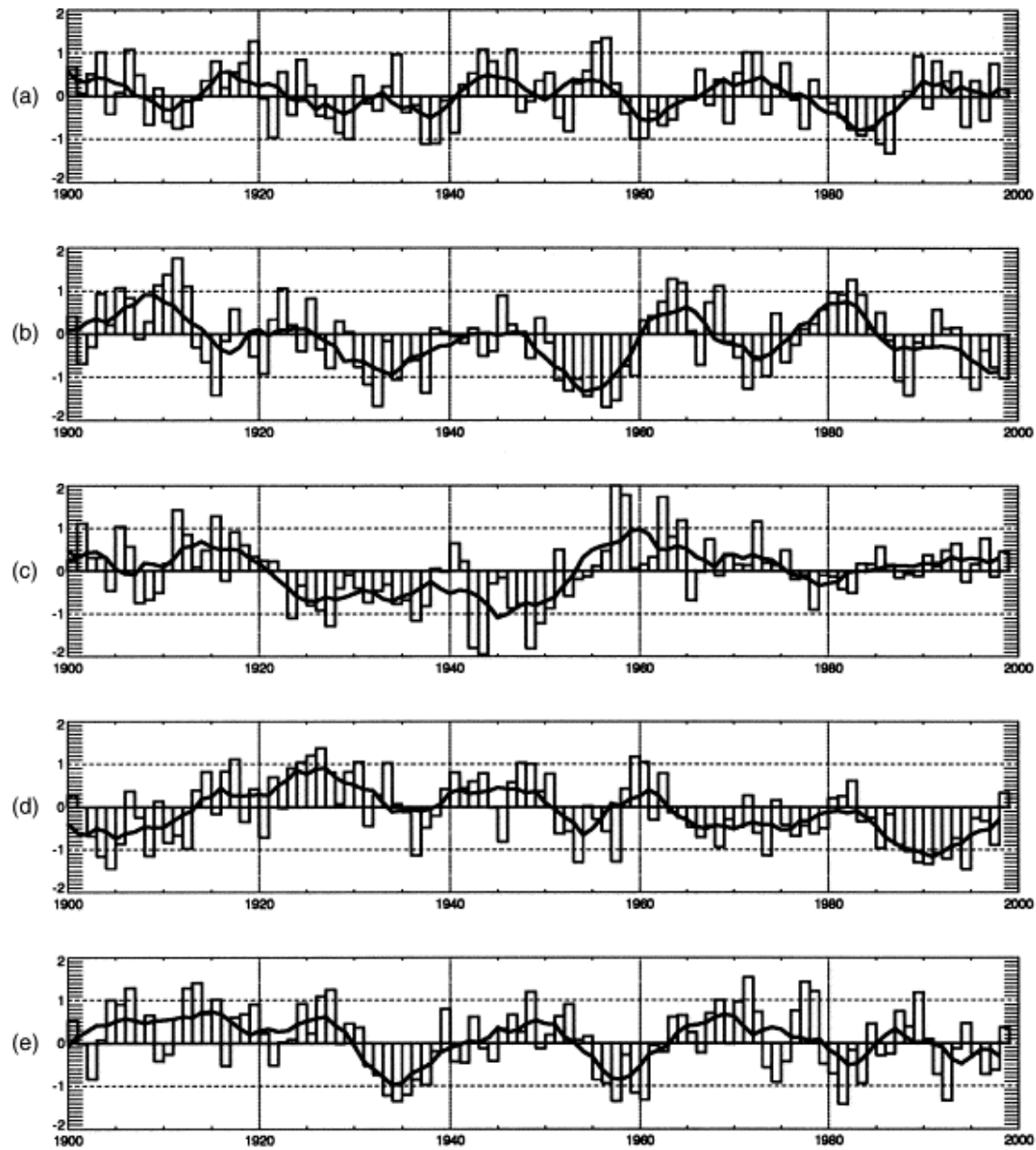


Fig. 17. SST anomaly spectrum at weather ship I (59°N , 19°W) for the period 1949–1964, with 95% confidence interval. The smooth curve was estimated from relation (24) using sensible and latent heat flux forcing only, and $\lambda = (4.5 \text{ month})^{-1}$ [after *Frankignoul and Hasselmann, 1977*].



Pierce 2001

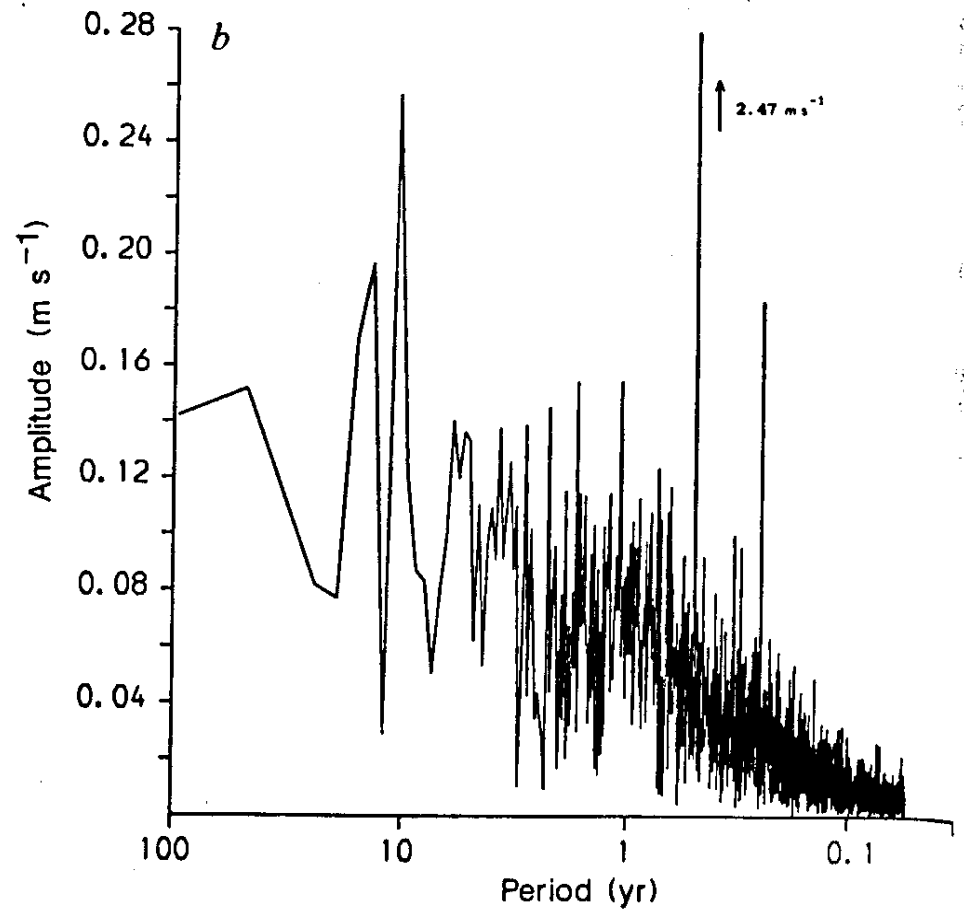
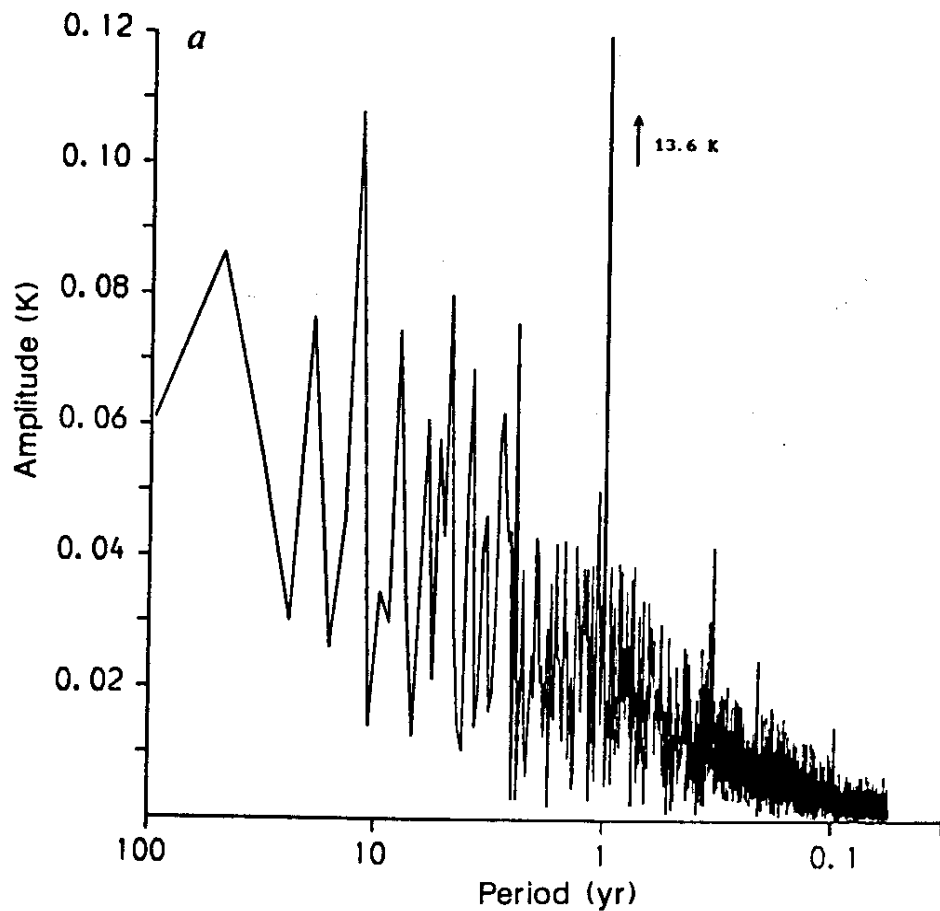


FIG. 2 Spectrum of the time variations of two selected spherical harmonic coefficients during the last 96 years of the model integrations. *a*, The Y_1^0 temperature coefficients, averaged with respect to pressure, giving the

mean pole-pole temperature difference. *b*, The Y_1^0 vorticity coefficient, averaged with respect to pressure, giving the mean solid-body rotation component of the atmospheric motion relative to the Earth.

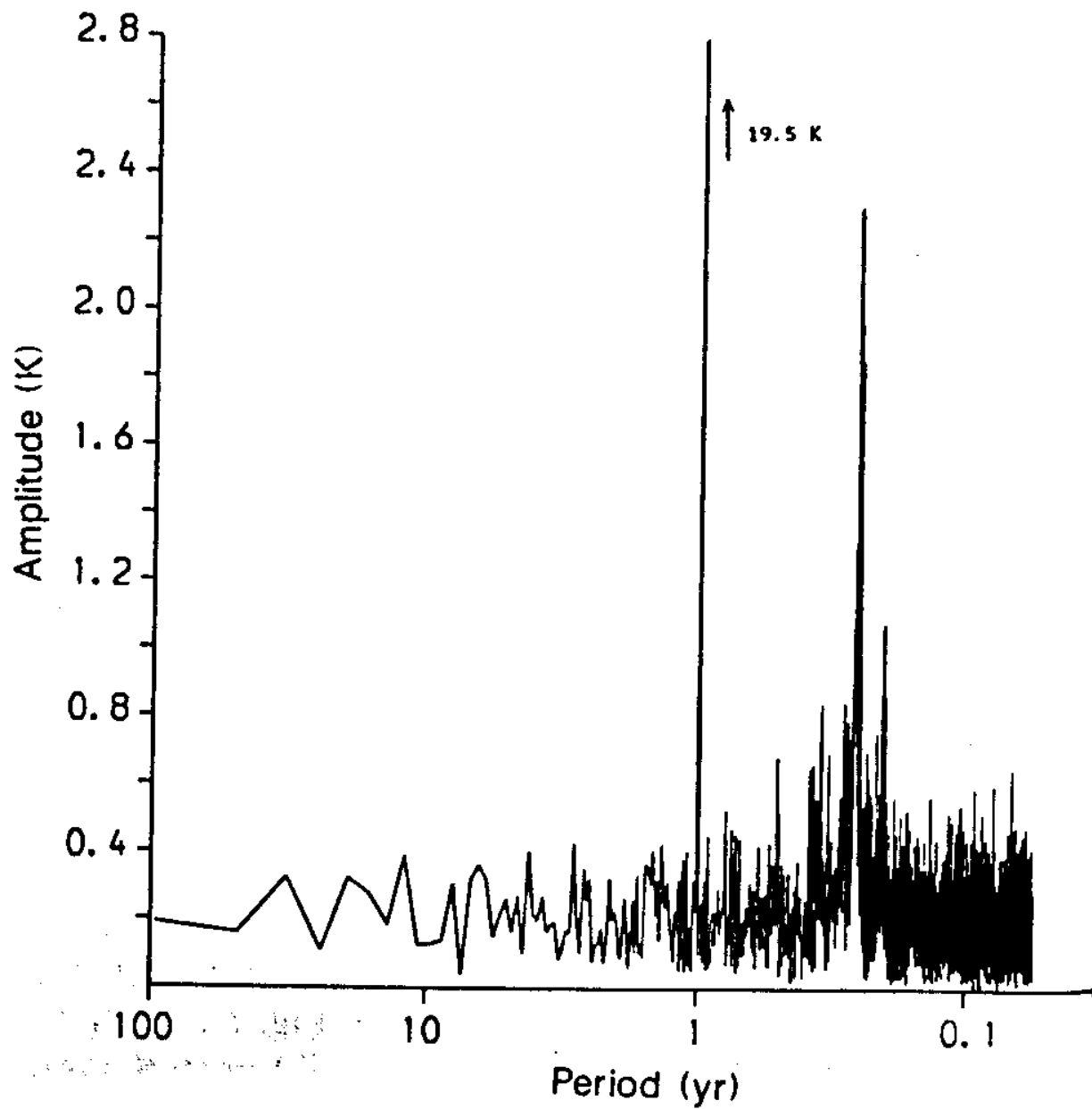


FIG. 3 Spectrum of the time variations of the surface temperature at a grid point at 47°N in the model.

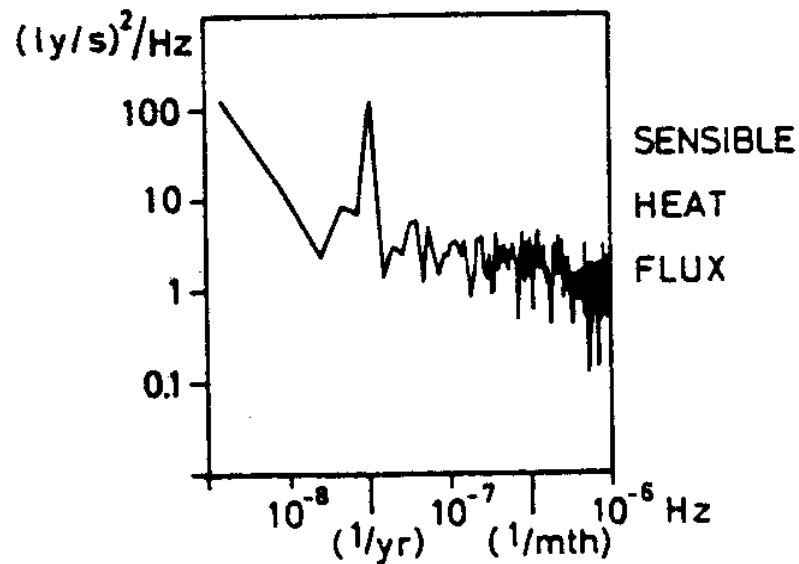
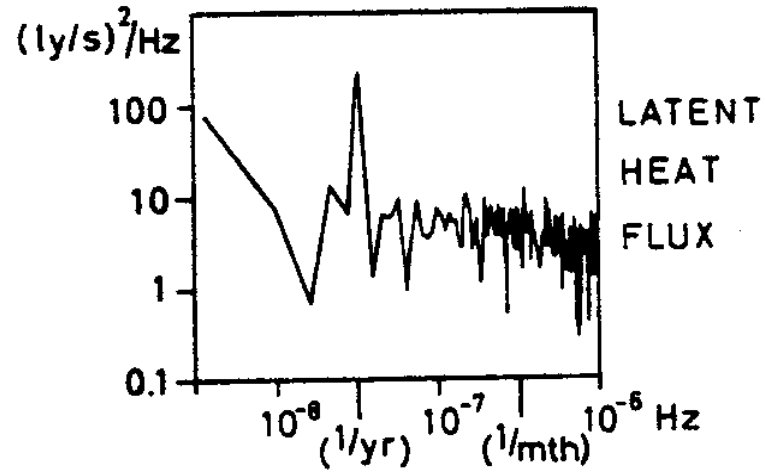


Fig. 6. Spectra of latent and sensible heat flux at Ocean Weather Ship India for the period 1949–1964 (after Frost, 1975).

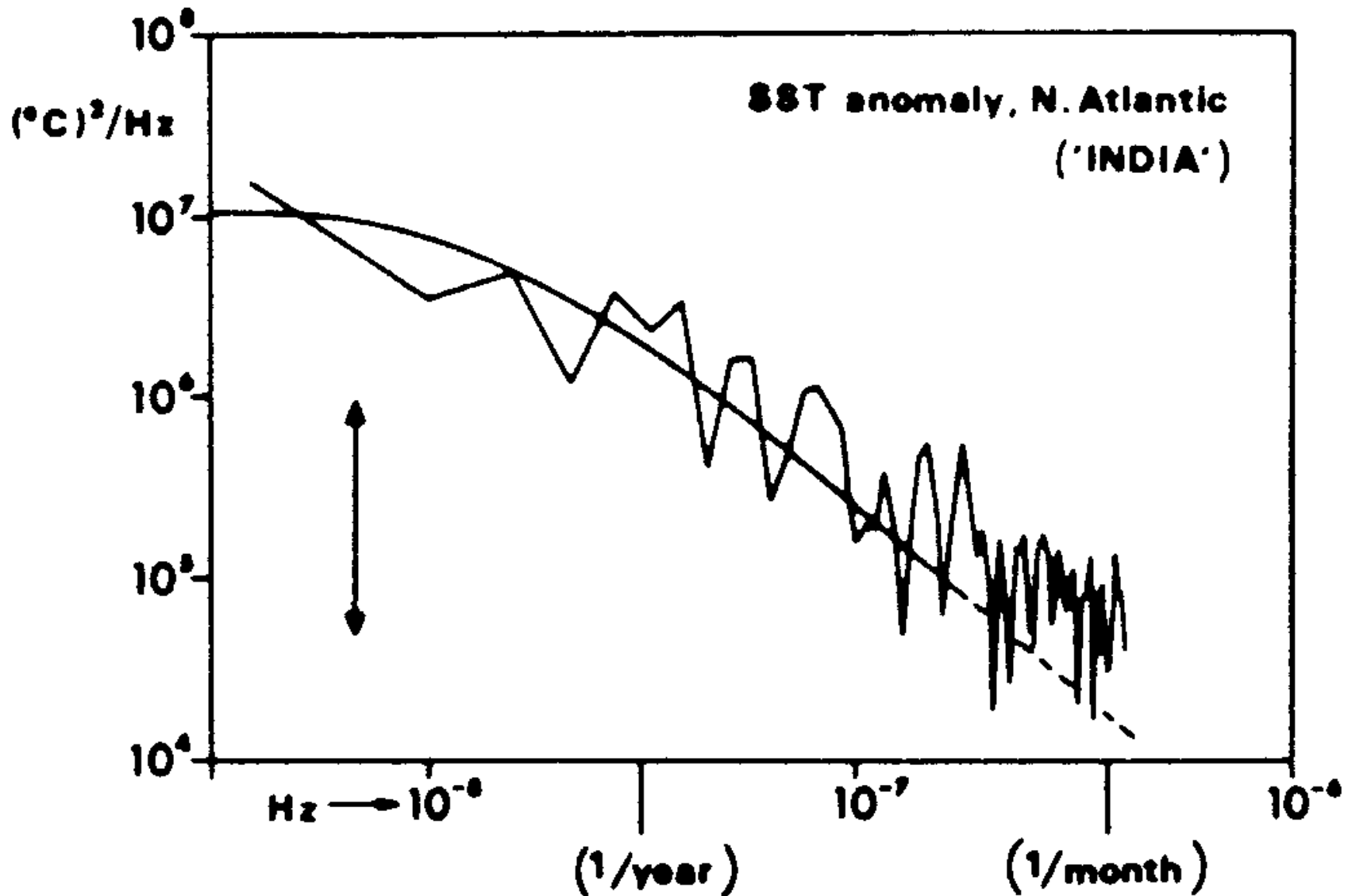
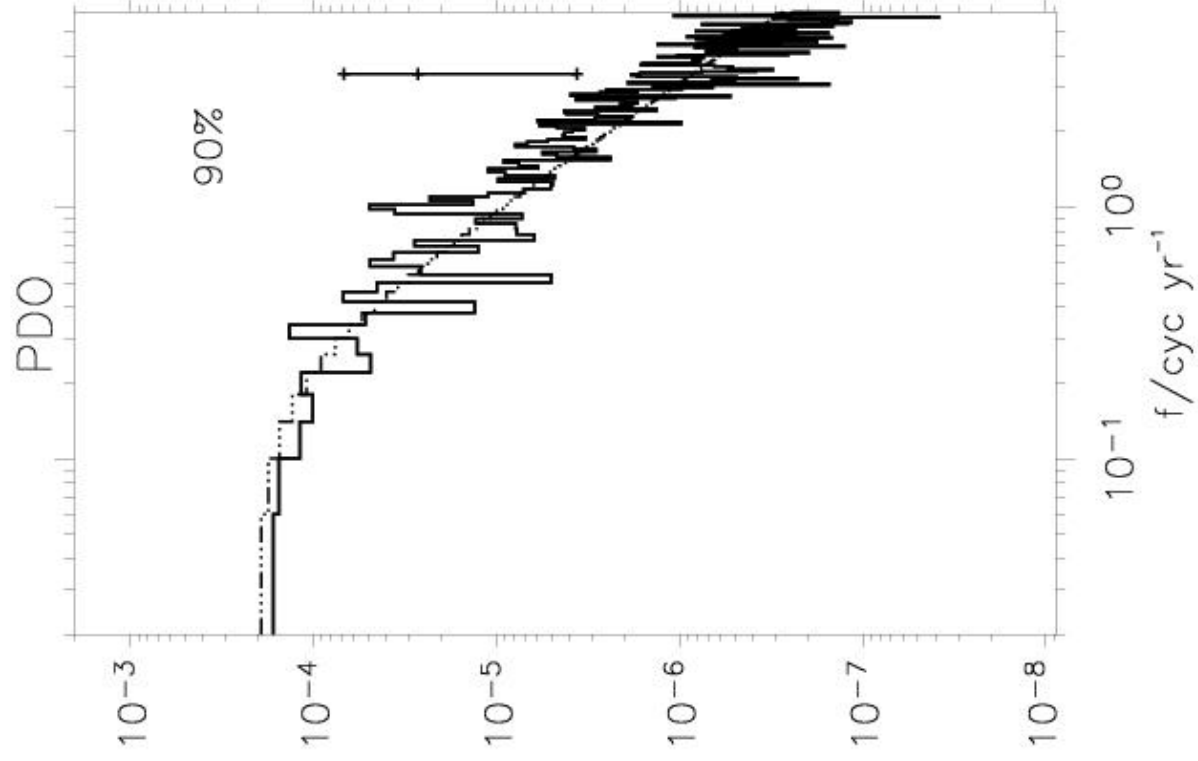
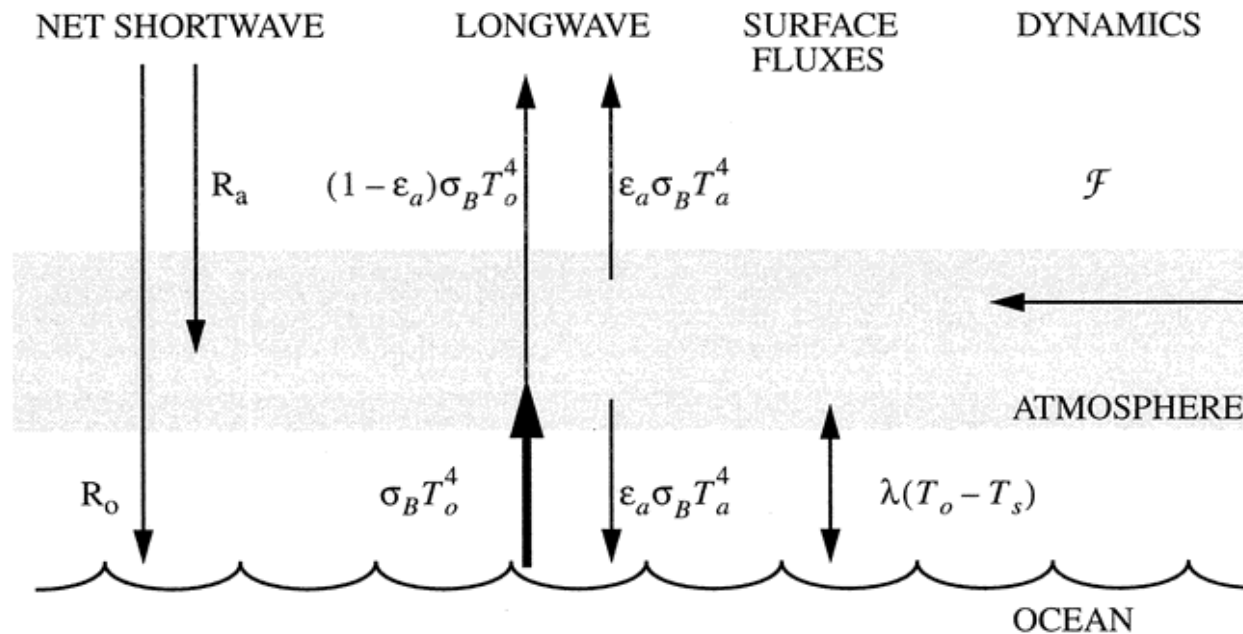


Fig. 17. SST anomaly spectrum at weatherstation I (59°N , 19°W) for the period 1949–1964, with 95% confidence interval. The smooth curve was estimated from relation (24) using sensible and latent heat flux forcing only, and $\lambda = (4.5 \text{ month})^{-1}$ [after *Frankignoul and Hasselmann, 1977*].



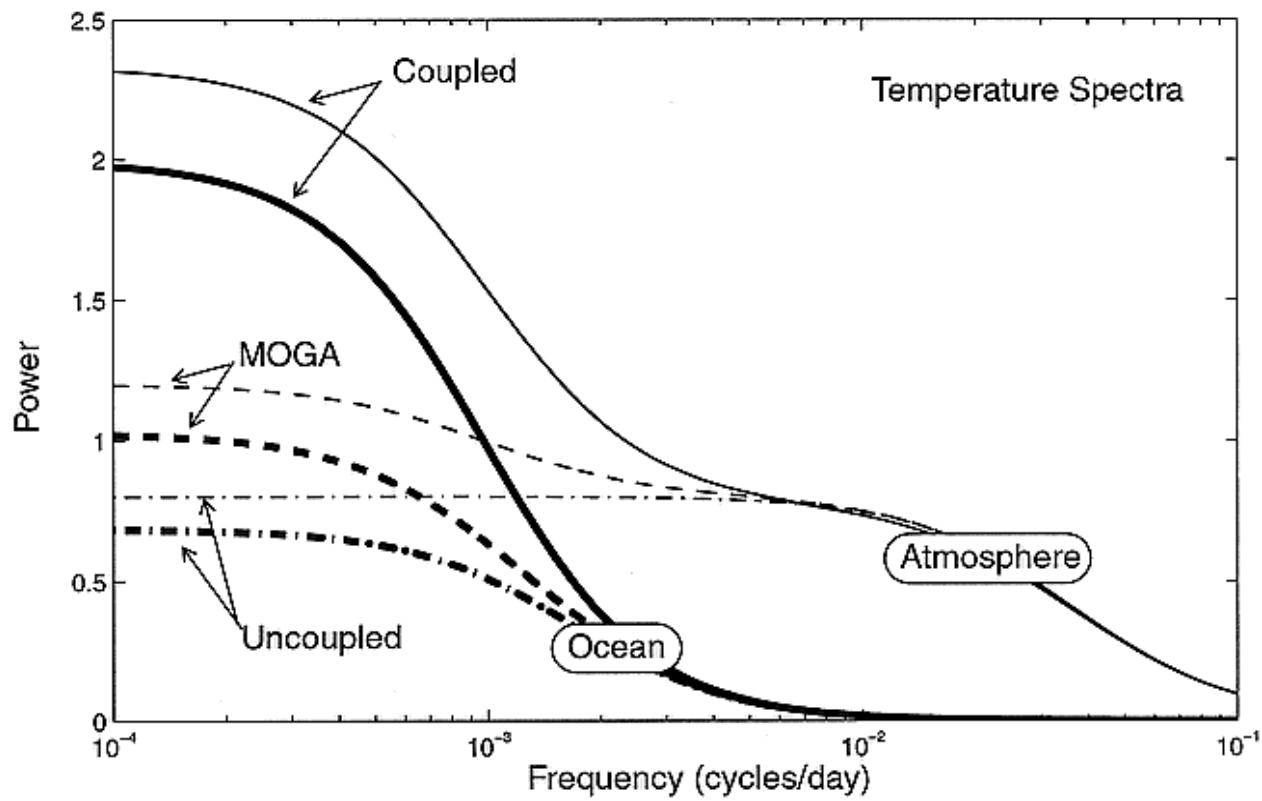
Ocean-Atmosphere Thermal Coupling

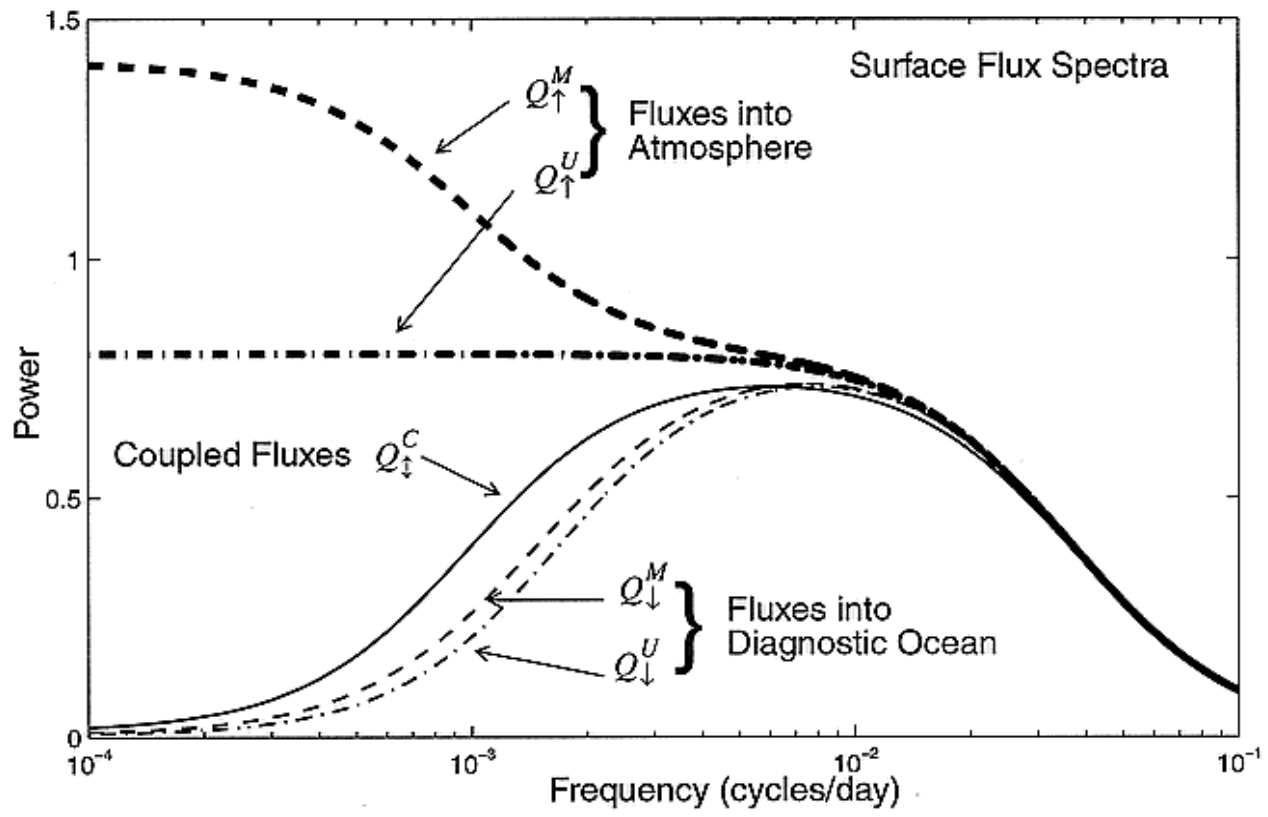
Barsugli and Battisti (JAS, 1998) model

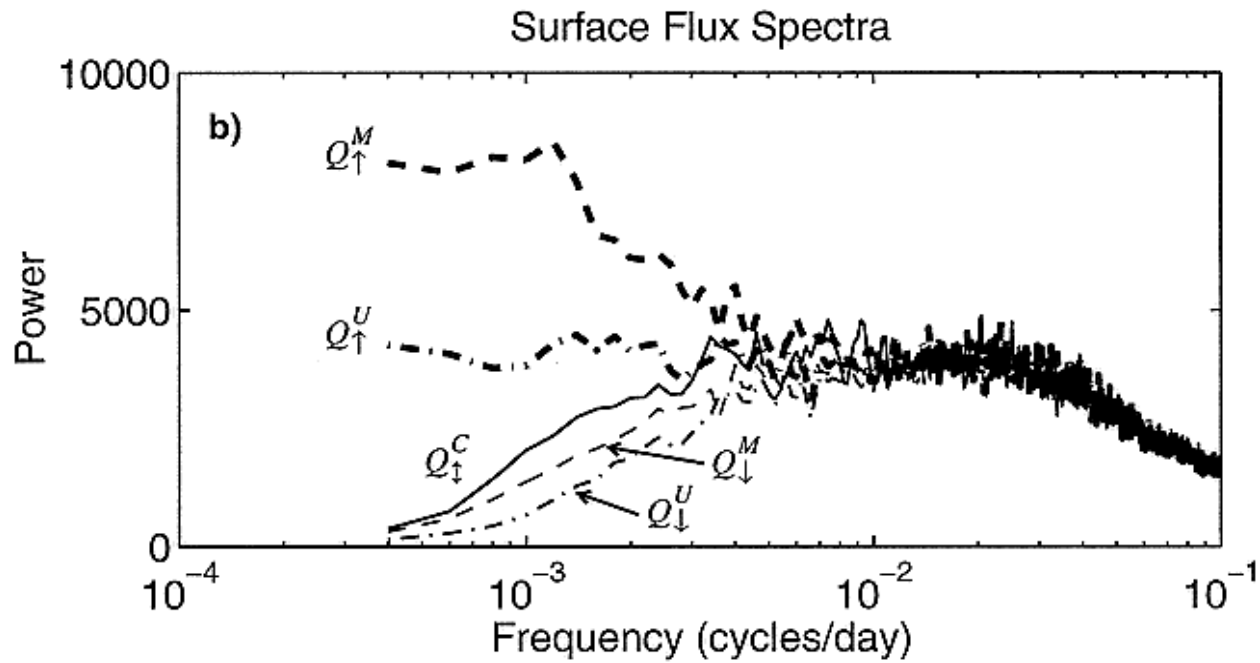
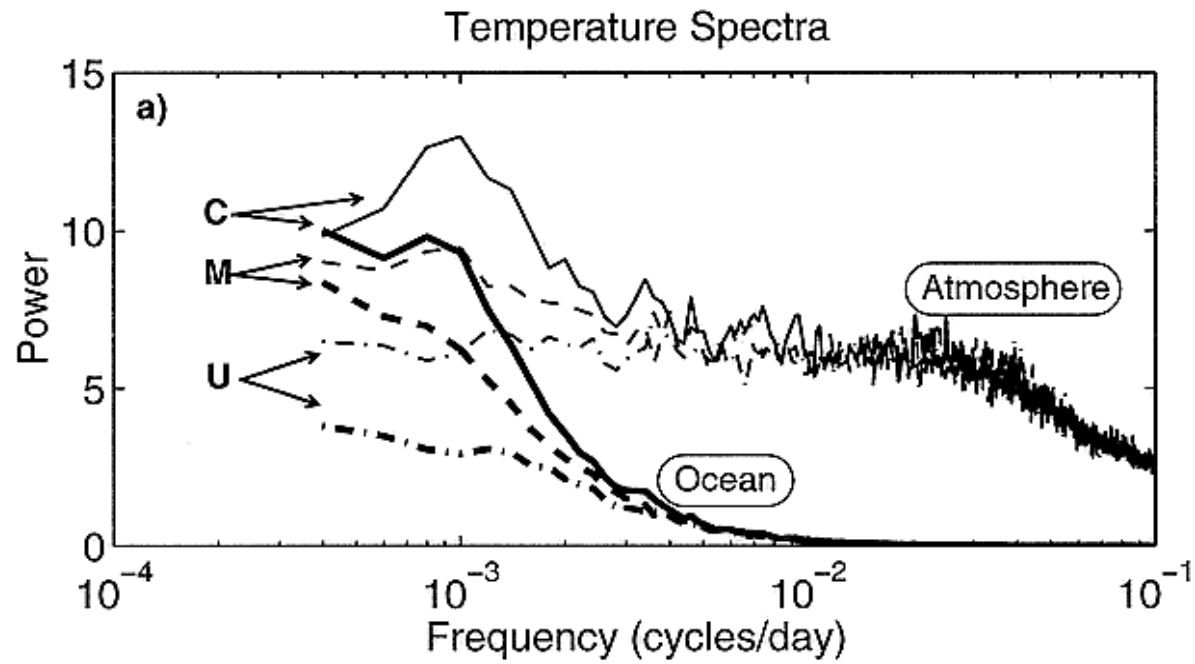


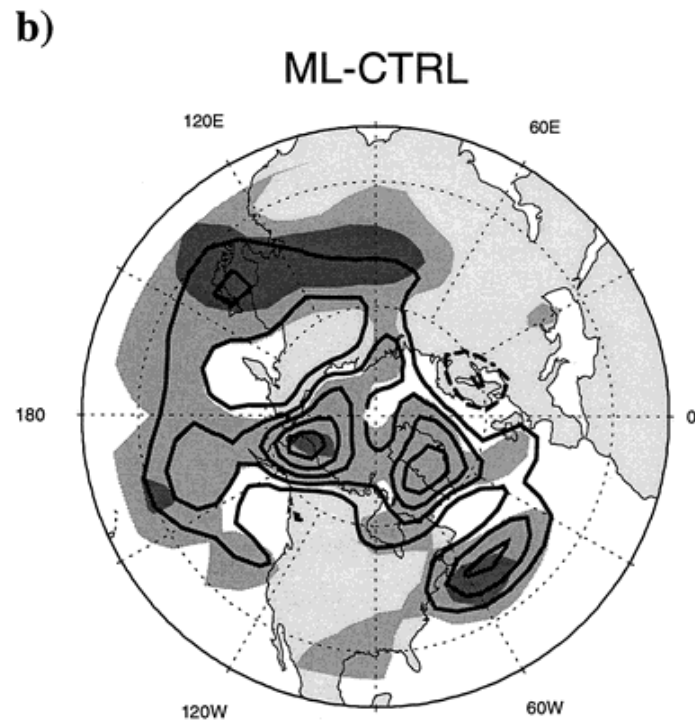
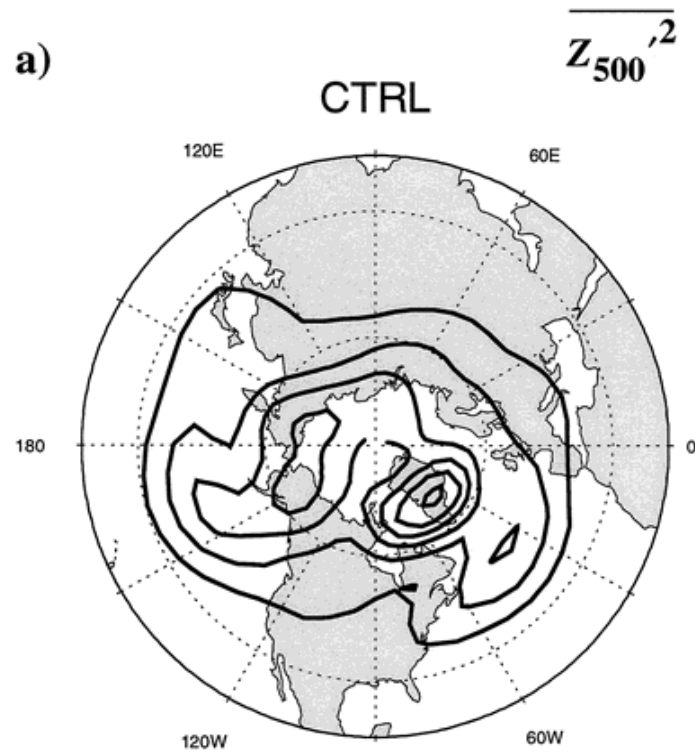
$$\gamma_a \partial_t T_a = -\lambda_{sa}(T_s - T_o) - \lambda_a T_a + F$$

$$\gamma_o \partial_t T_o = -\lambda_{so}(T_s - T_o) - \lambda_o T_o$$

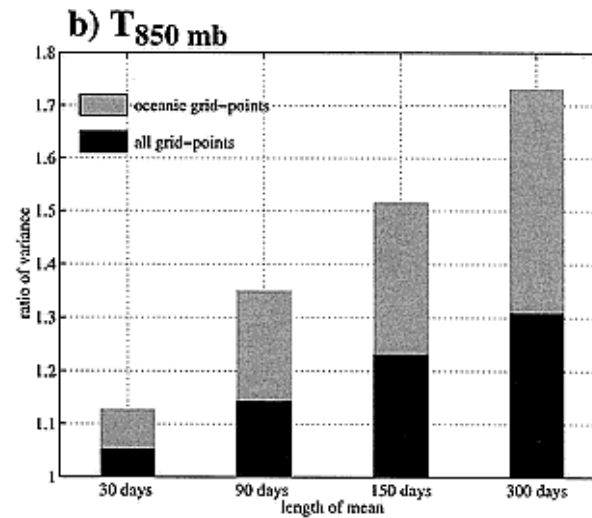
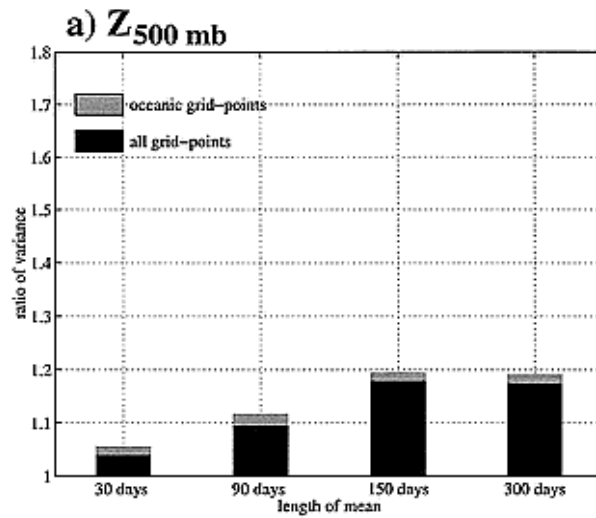


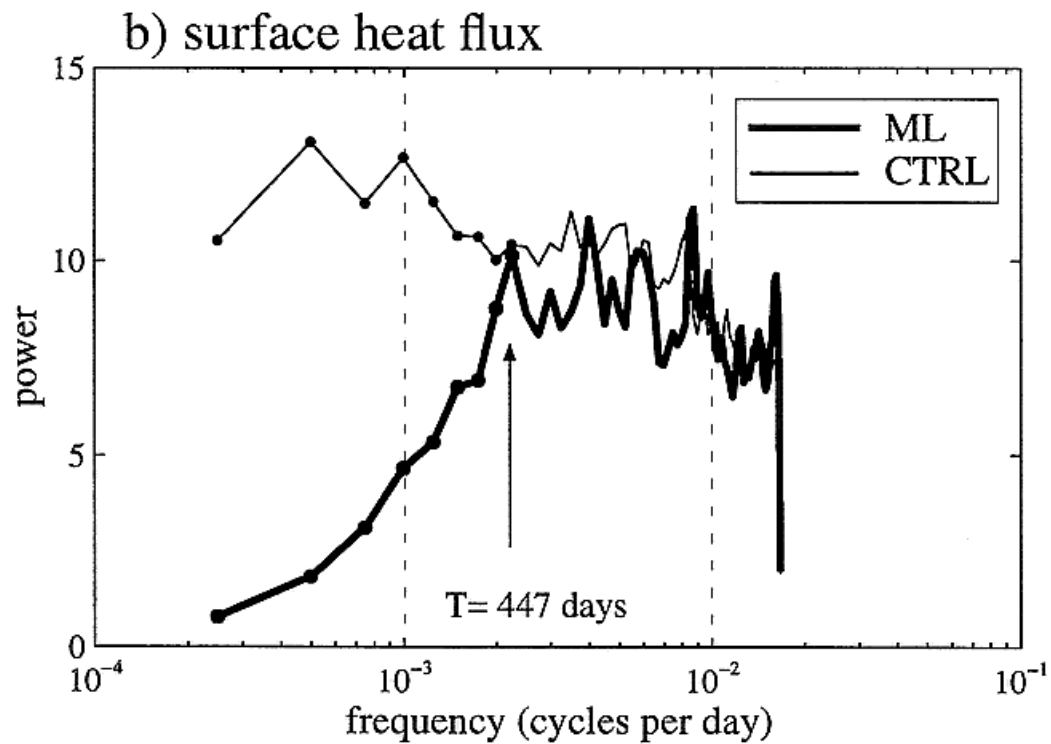
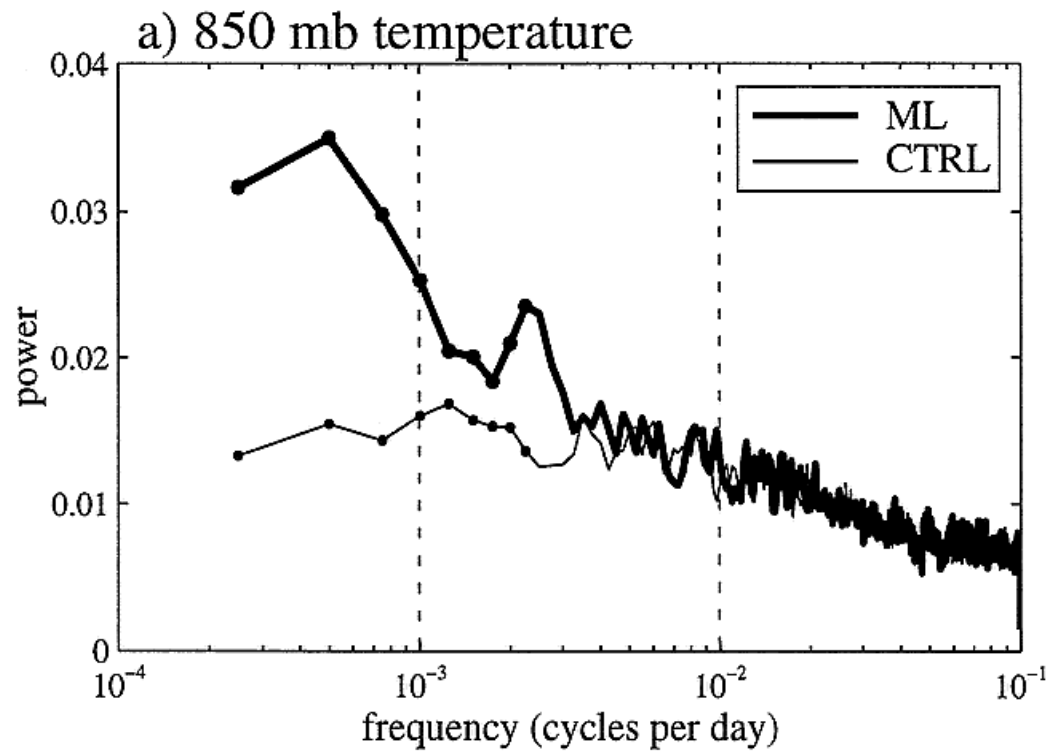






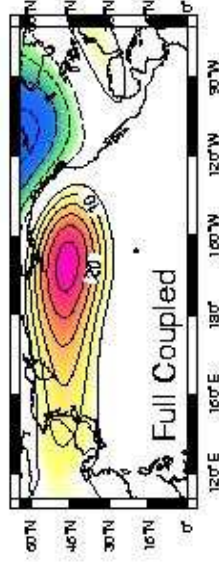
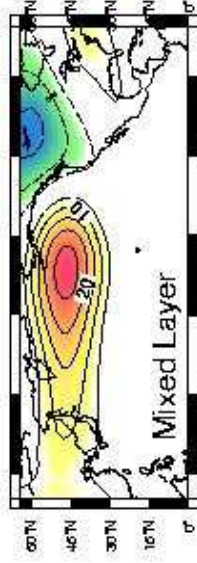
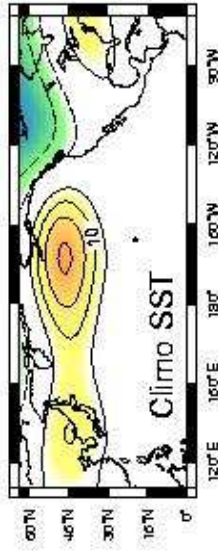
ML to CTRL ratio of integrated NH variance



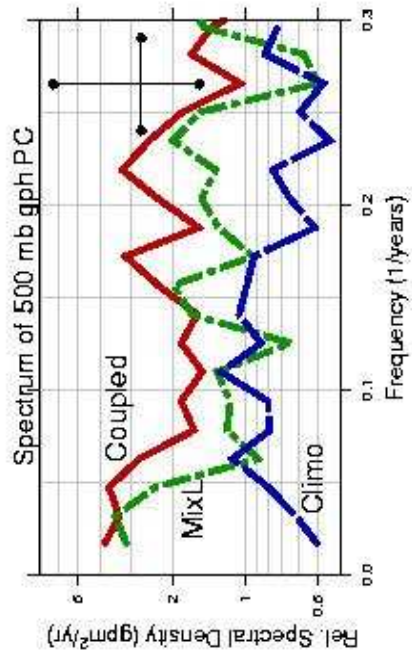
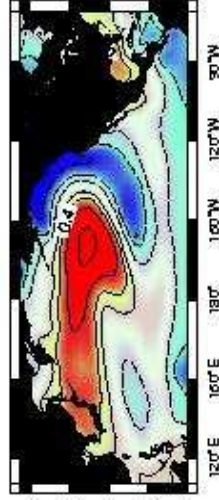
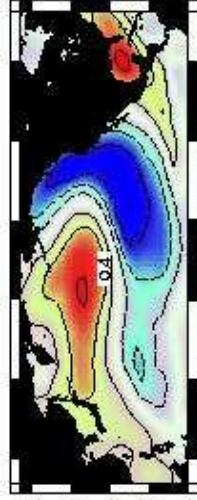


Leading mode of N. Pacific Variability, CCM3

EOF #1, 500 mb gph anom



Correlation of SSTA with PC

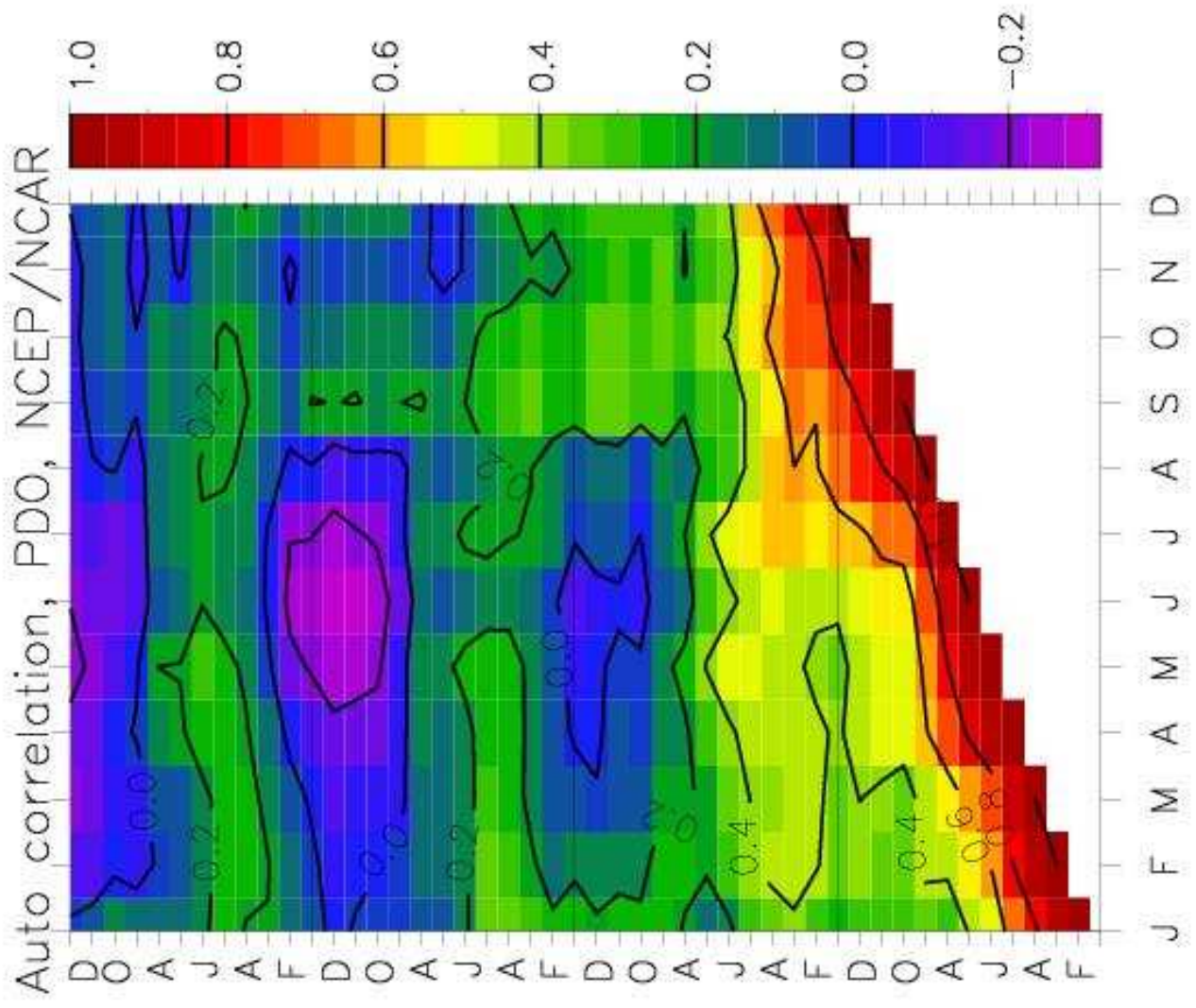


Basic effect of atmosphere-ocean thermal coupling:

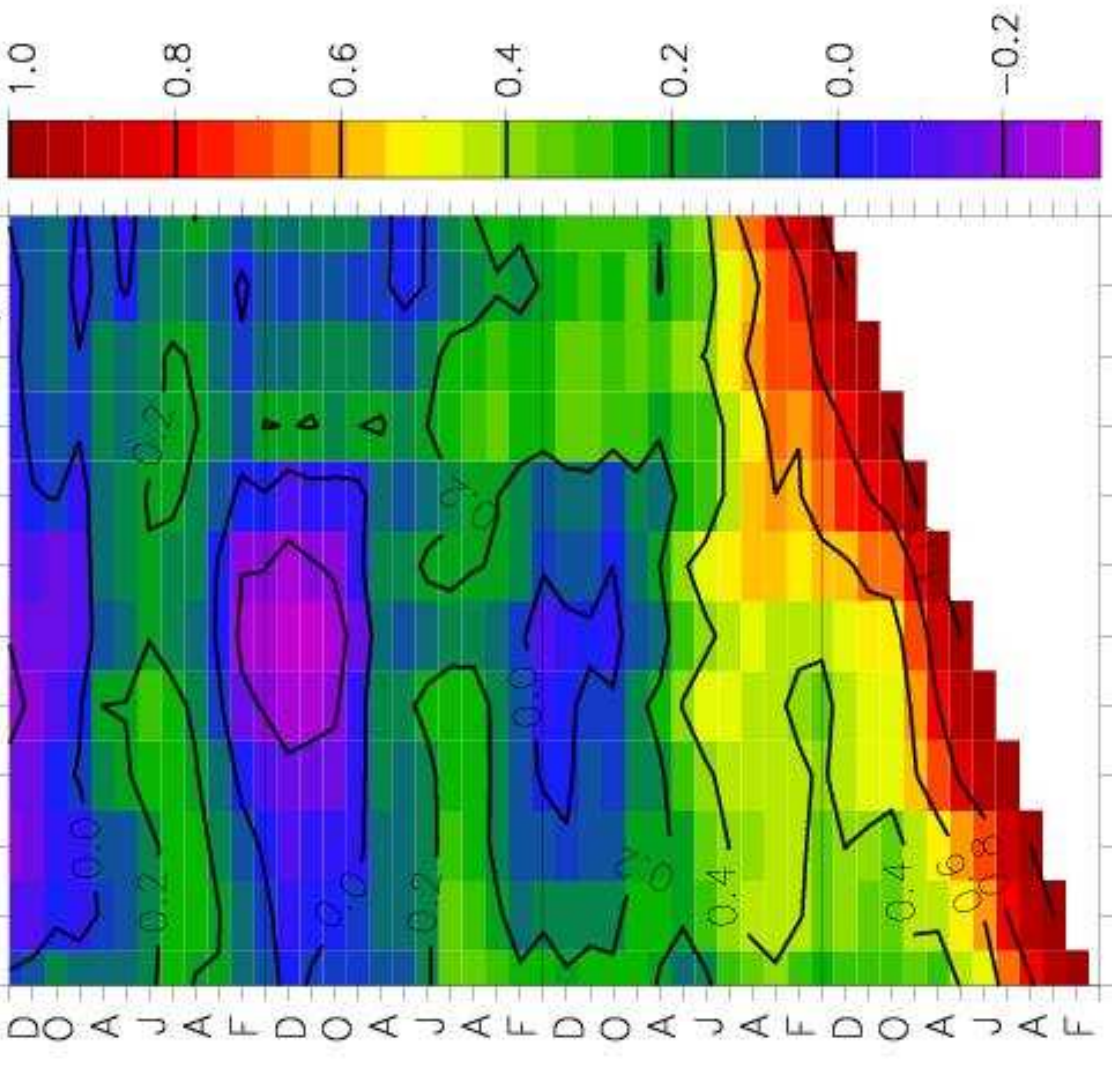
- increases variance in both media, while patterns are largely unchanged
- decrease energy flux between them
- prescribing SST does not yield the proper simulation of low frequency variance in the atmosphere (will yield the atmospheric mode least damped by the damping at the surface)

Processes contributing to increased persistence of SST: Reemergence

$$\frac{dT}{dt} = \frac{-\lambda T + F - e\Delta T}{h}$$



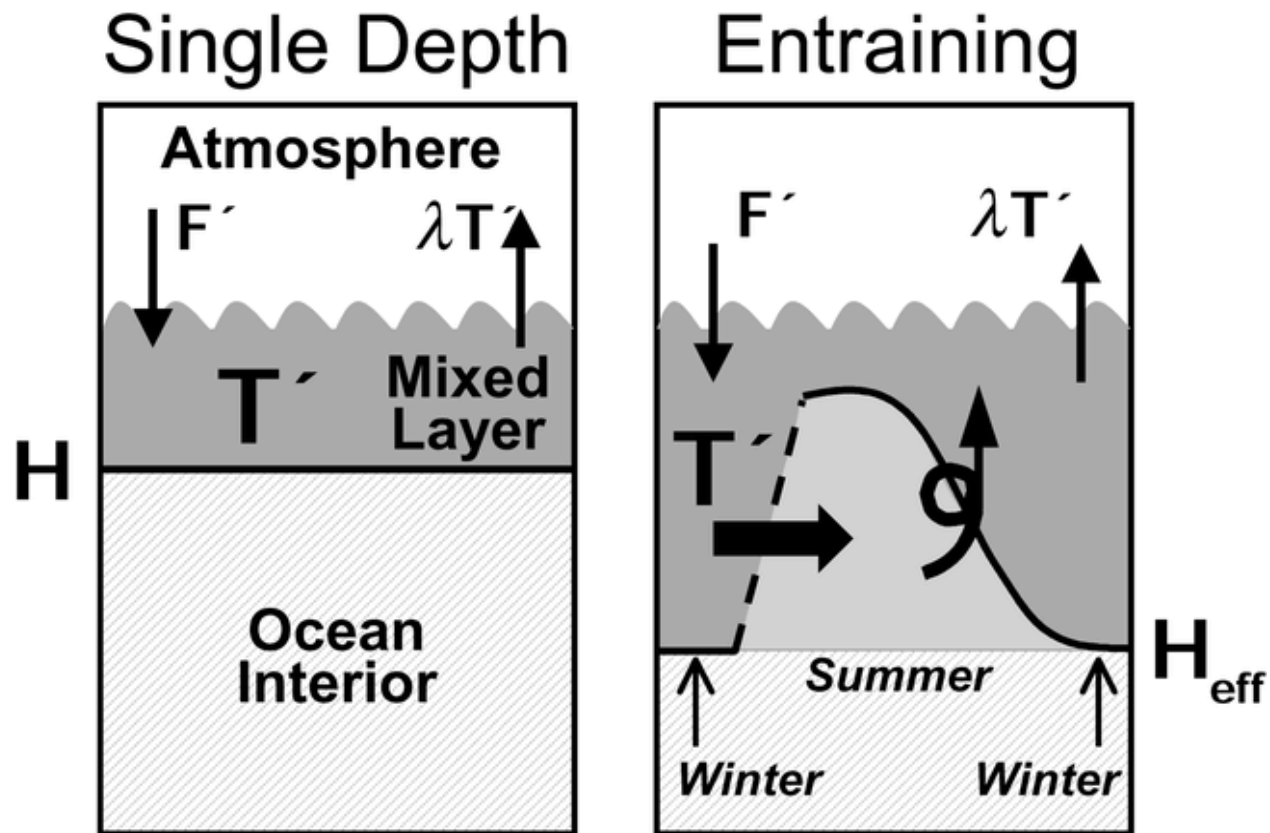
Auto correlation, PDO, NCEP/NCAR

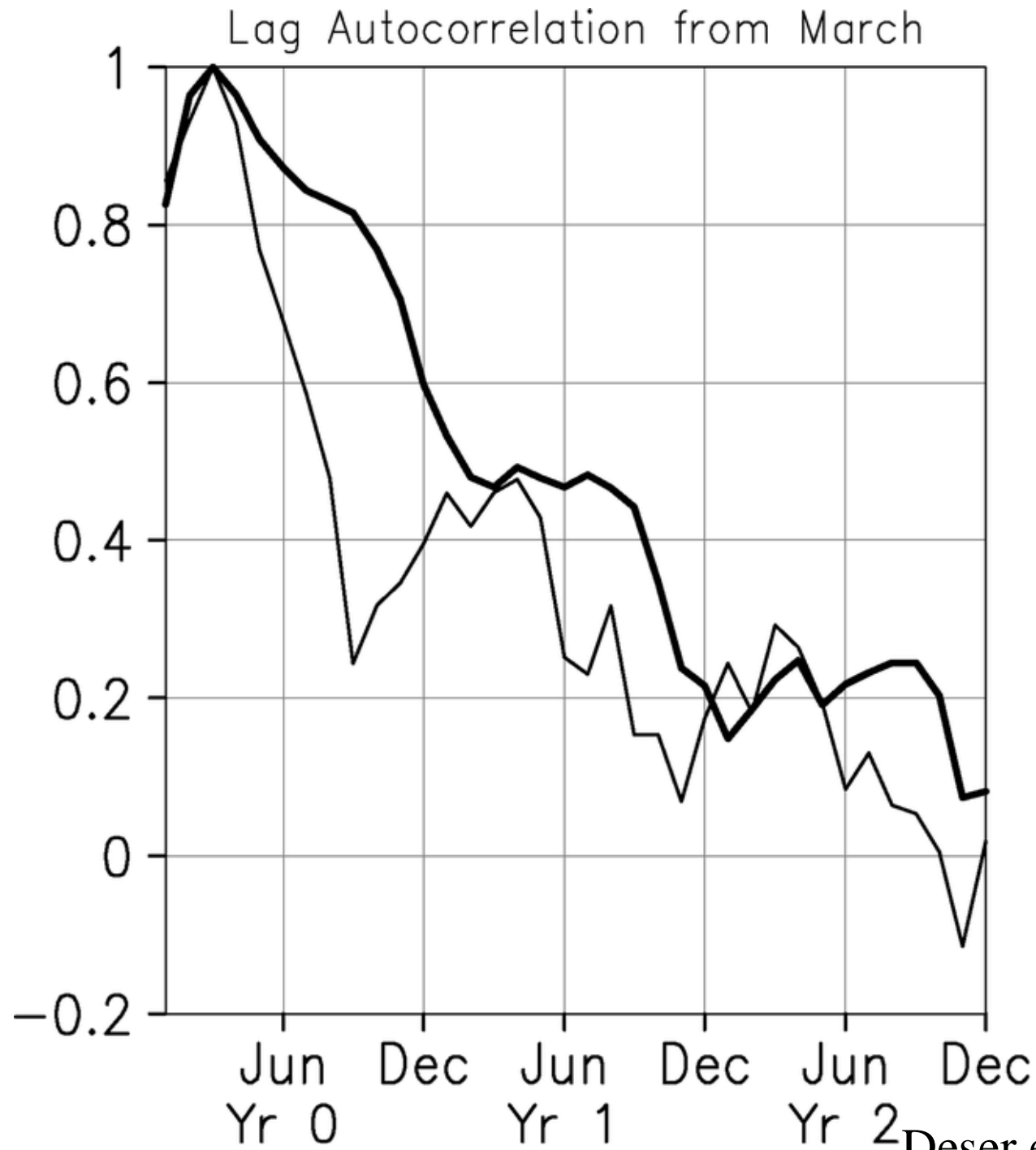


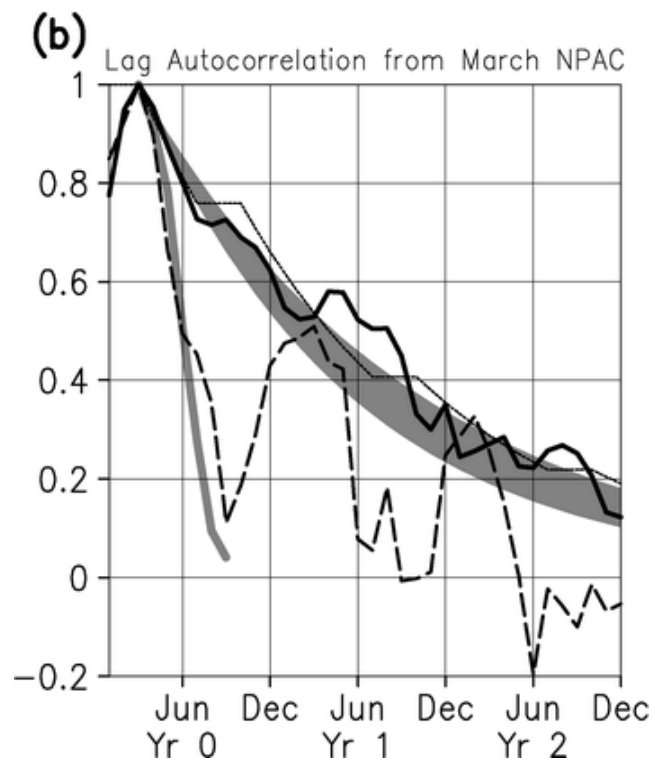
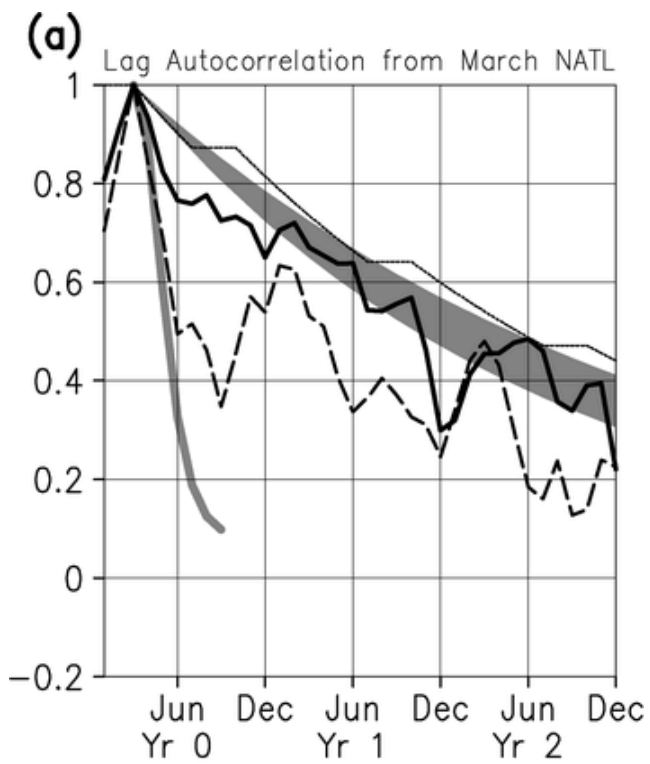
1.0
0.8
0.6
0.4
0.2
0.0
-0.2

D A J A F D O A J A F D O A J A F D O A J A F

J F M A M J J A S O N D







Deser et al. JC, 2003

Nonlocal Response to Stochastic Forcing

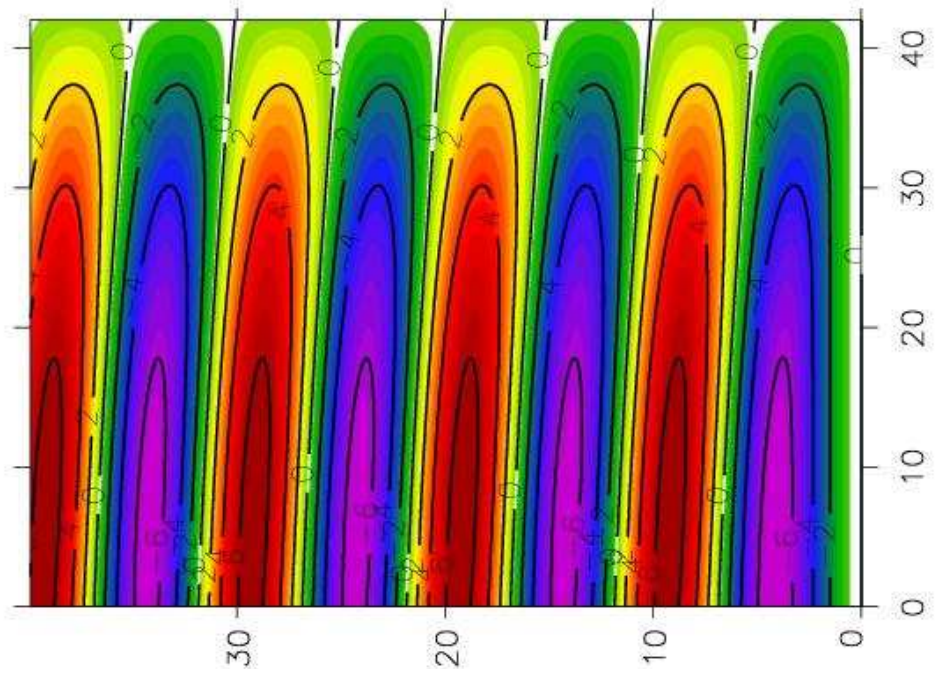
Stochastic forcing of ocean pressure or advected temperature

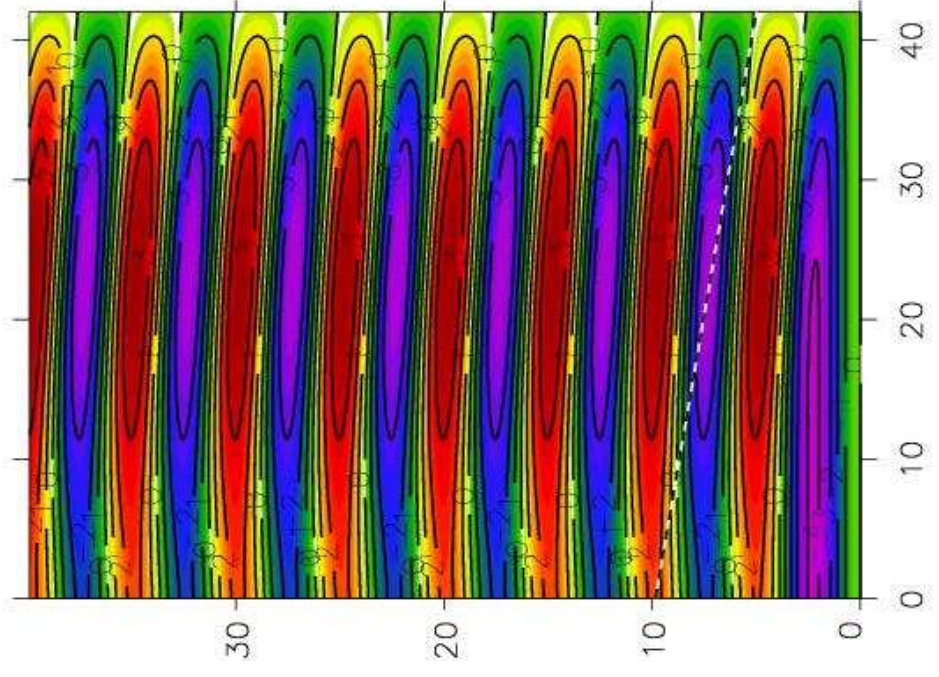
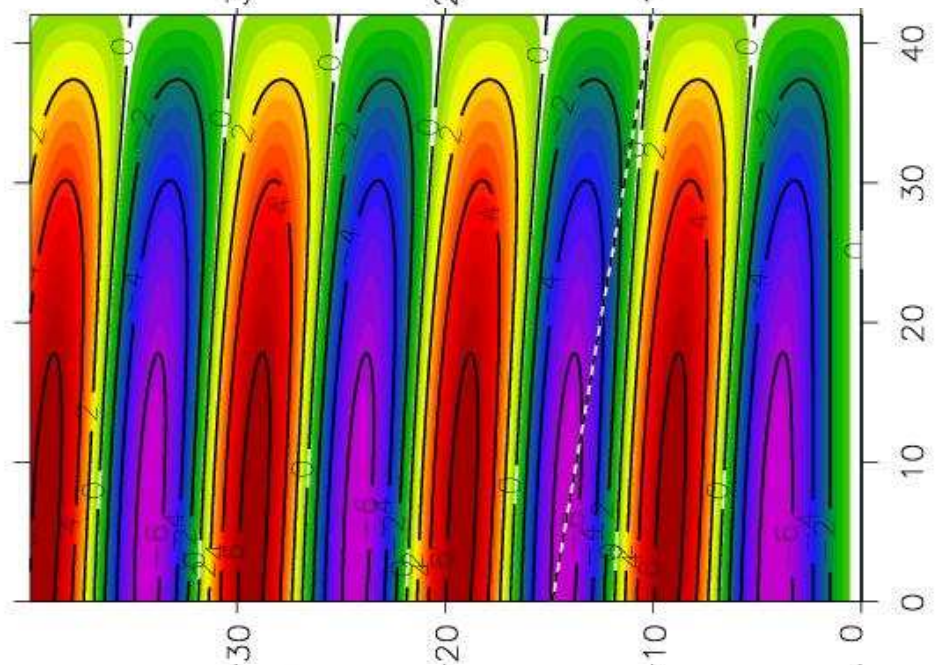
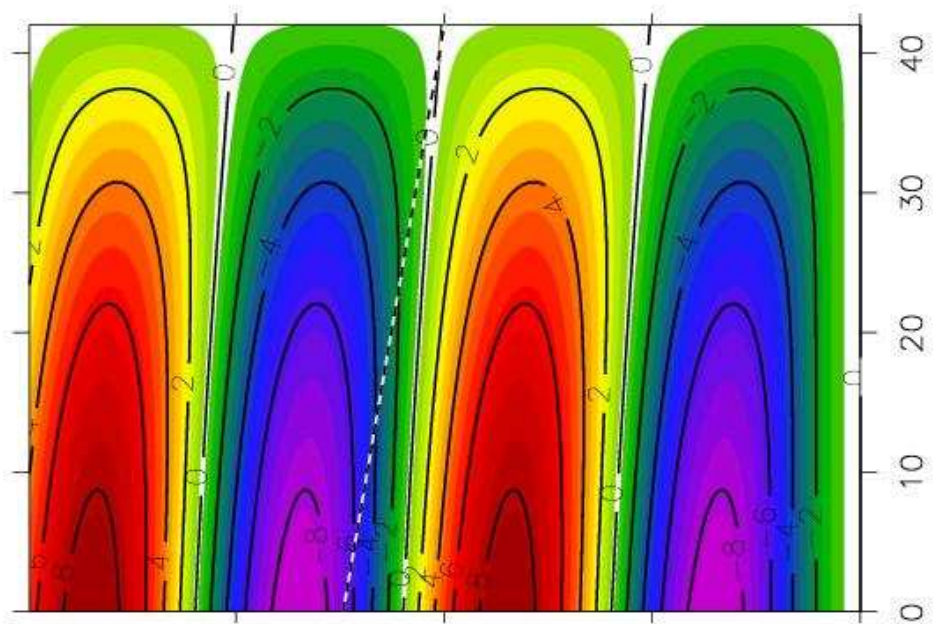
$$\partial_t T + u \partial_x T = F(x, t)$$

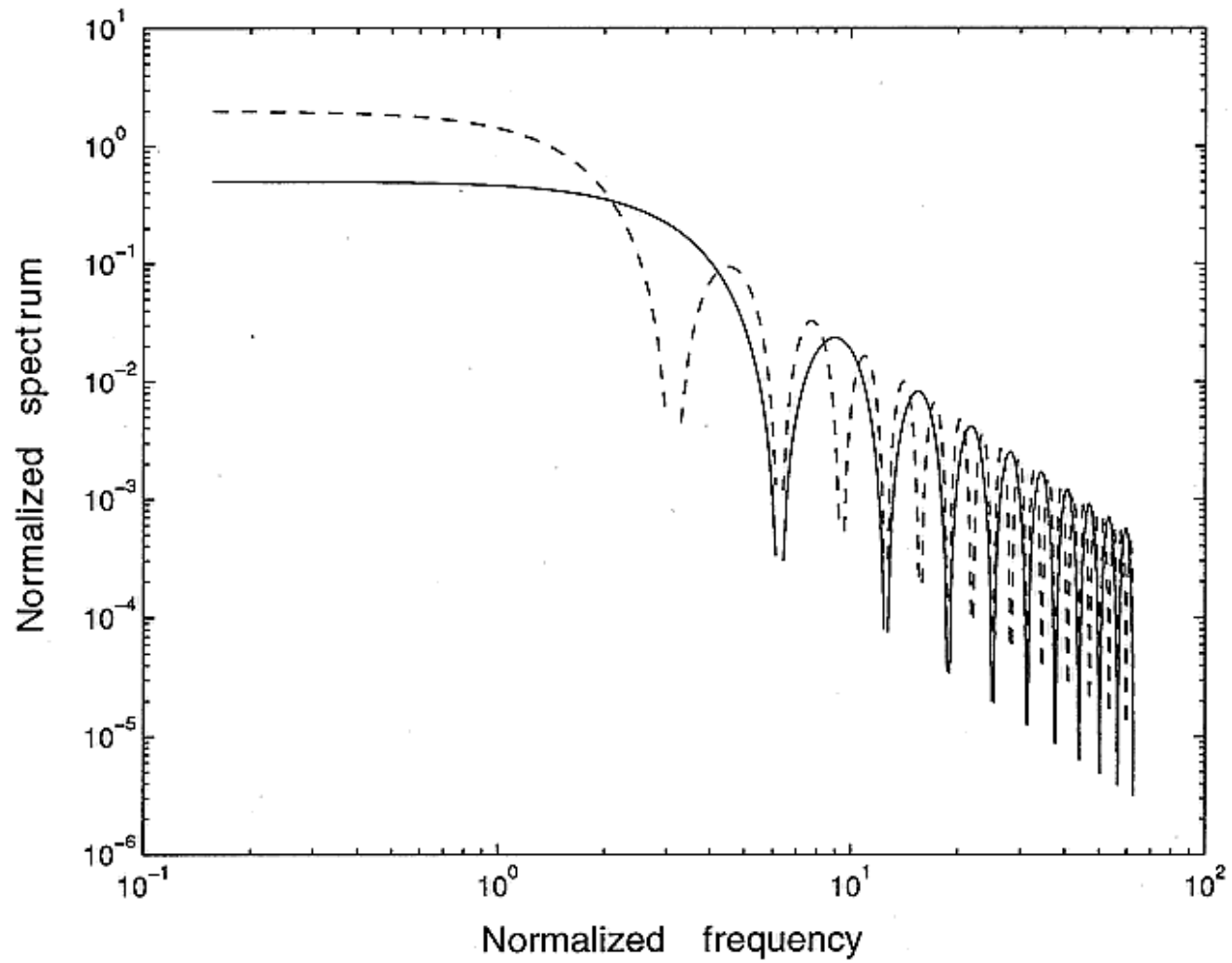
$$\partial_t P + c \partial_x P = F_{EK}(x, t)$$

$$P(x, t) = \int_{x_0}^x \frac{dx'}{c} F_{EK}(x', t - \frac{x - x'}{c}) + P(x_0, t - \frac{x - x_0}{c})$$

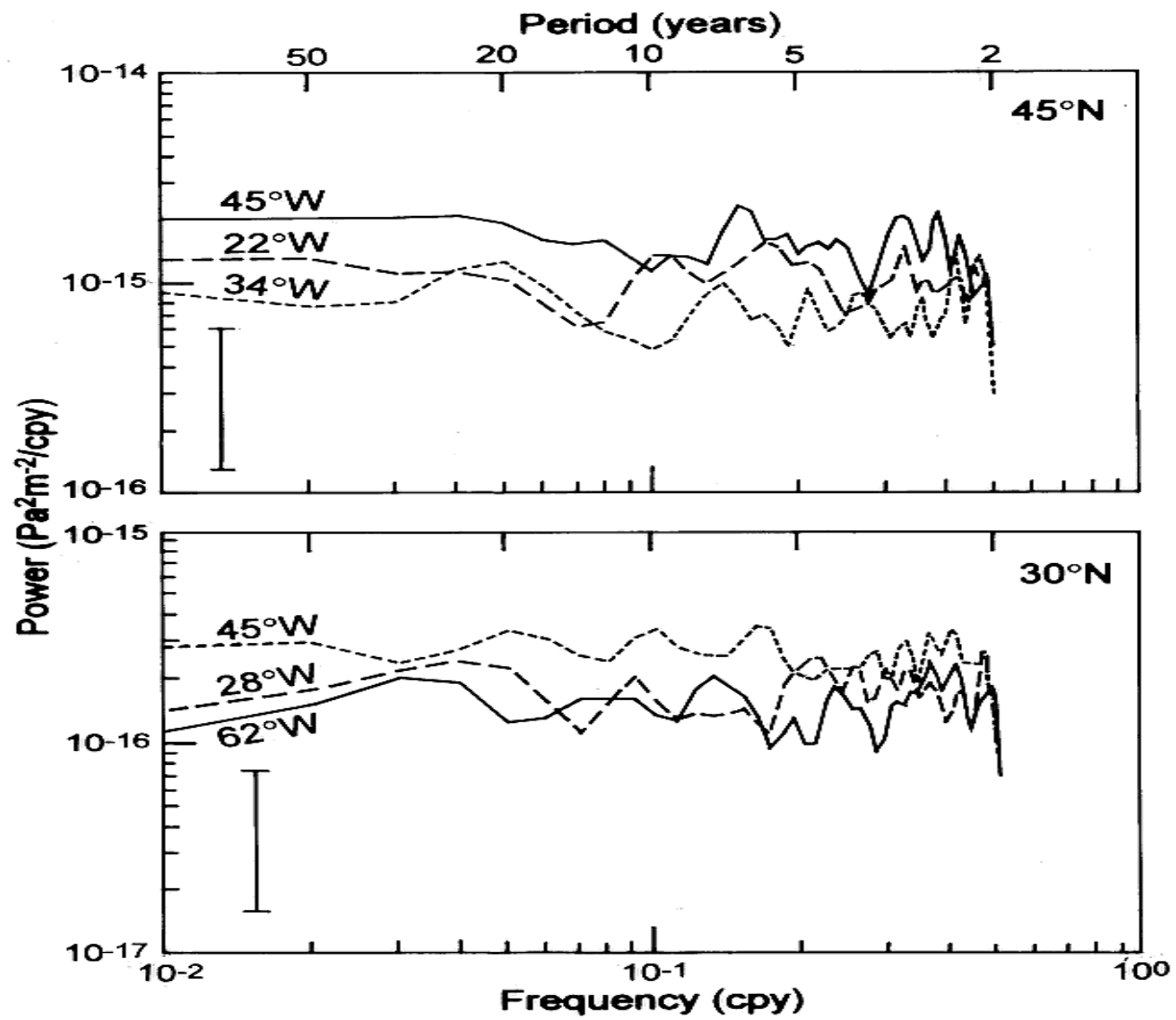
$$P(x, t) = \int_{t - \frac{x - x_0}{c}}^t dt' F_{EK}(x - c(t - t'), t') + P(x_0, t - \frac{x - x_0}{c})$$



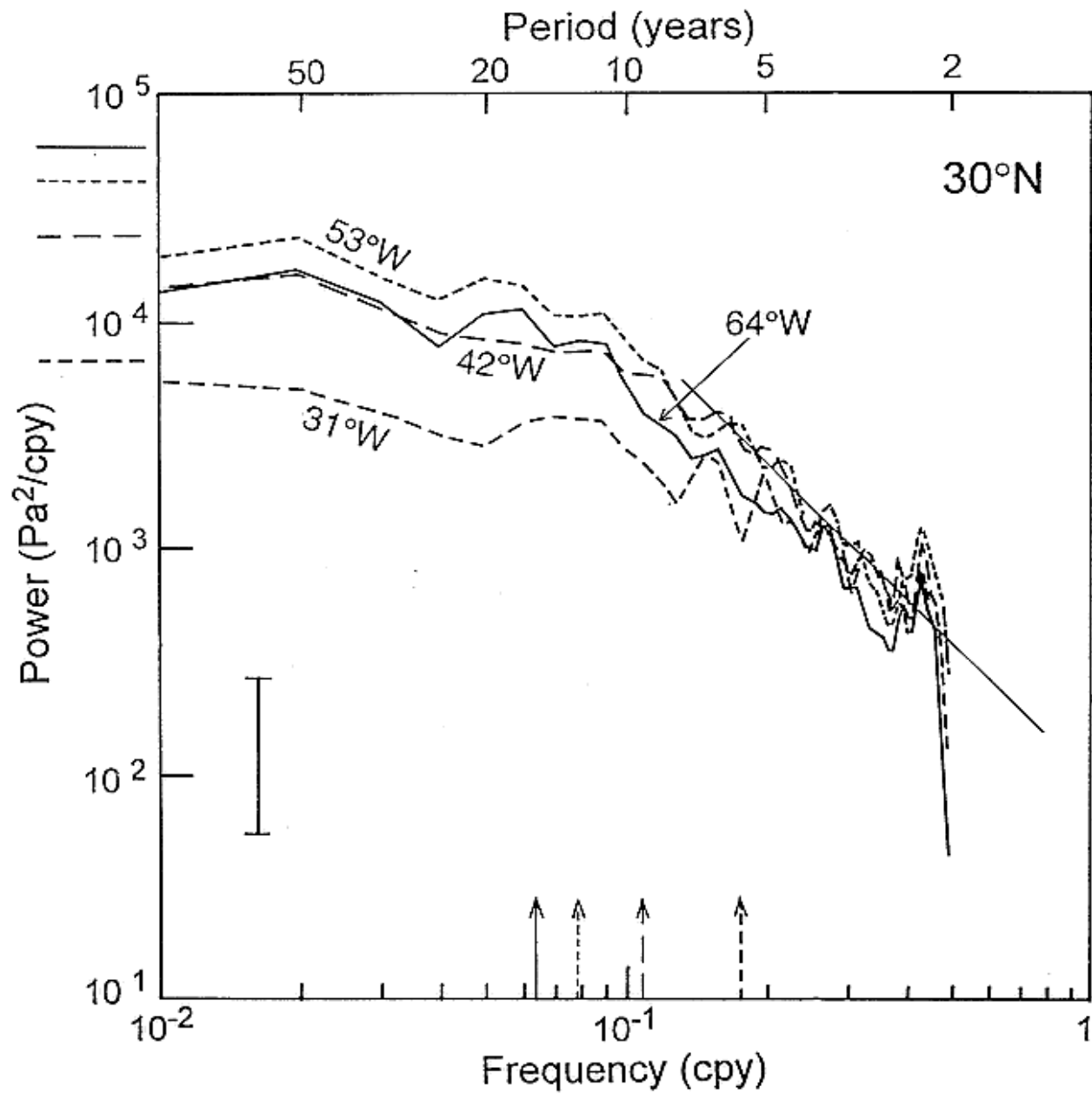




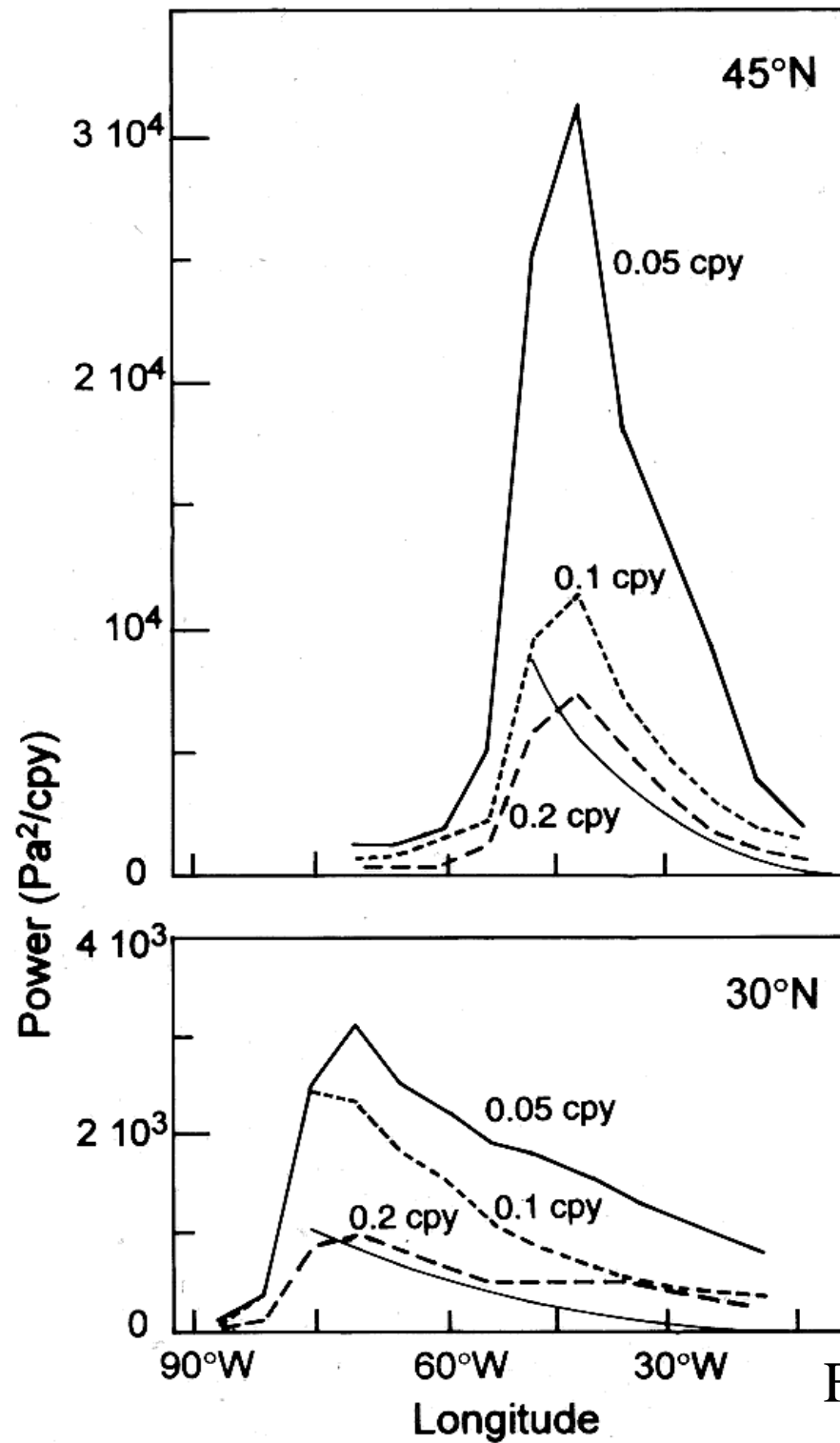
Frankignoul et al. 1997



Frankignoul et al. 1997

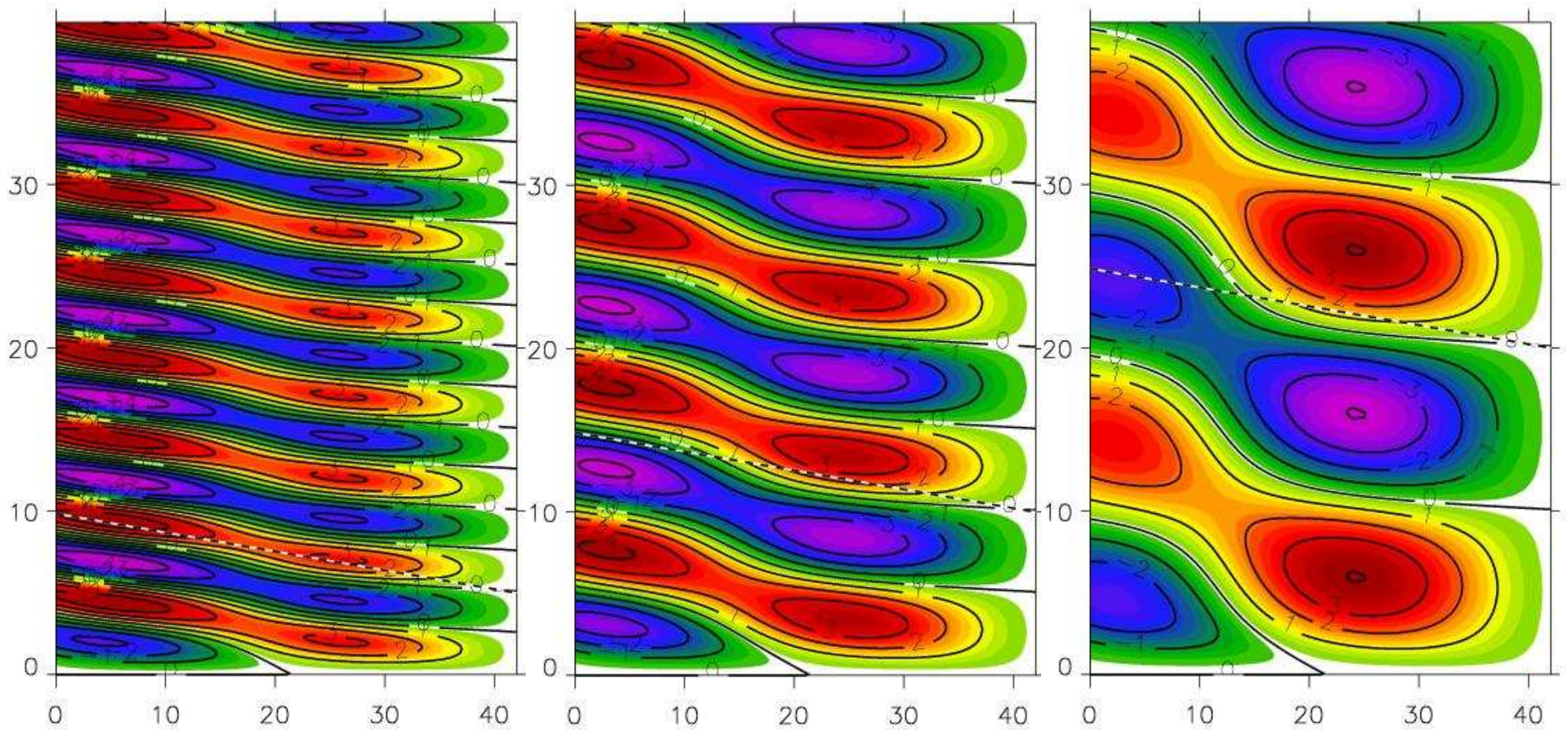


Frankignoul et al. 1997

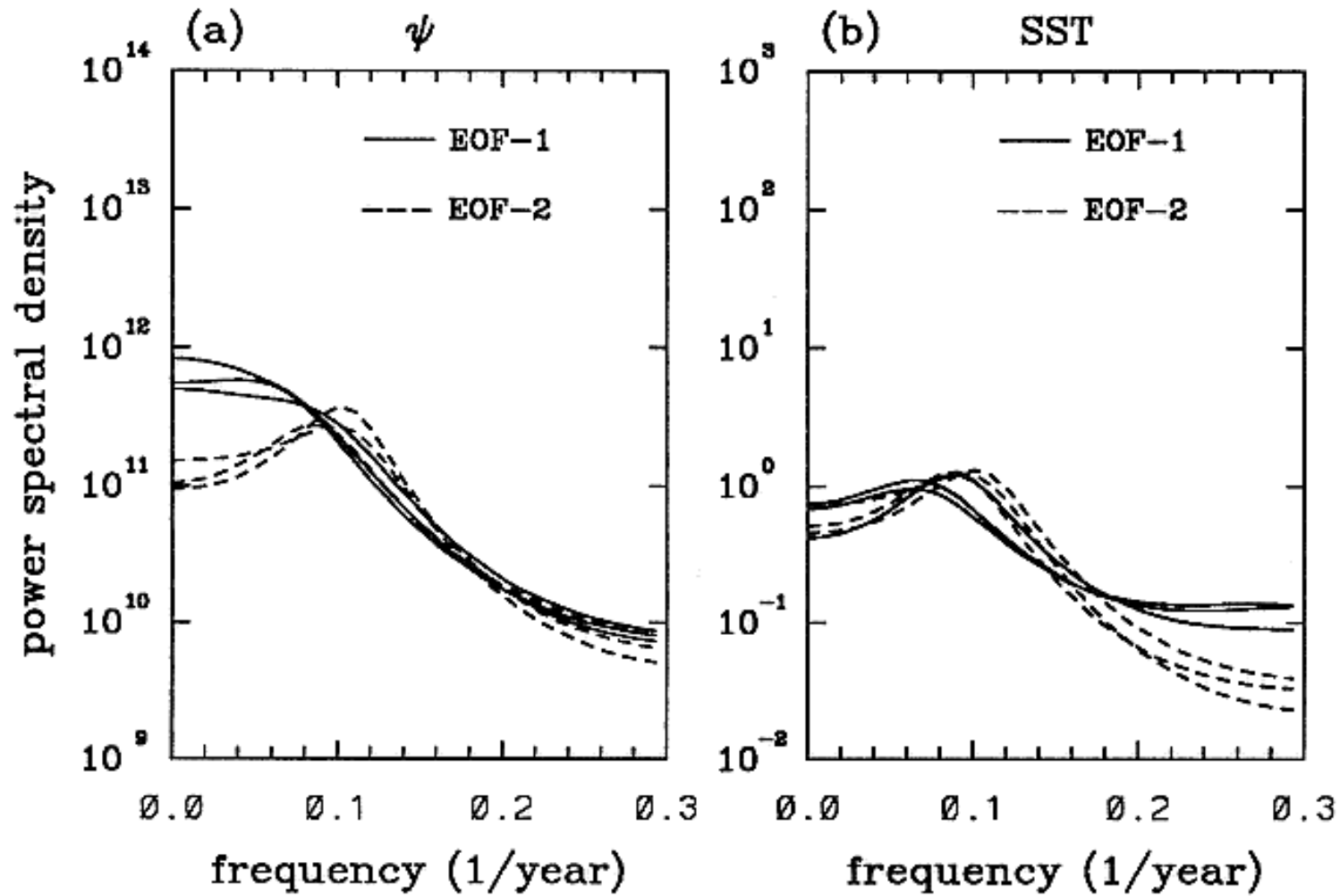


Frankignoul et al. 1997

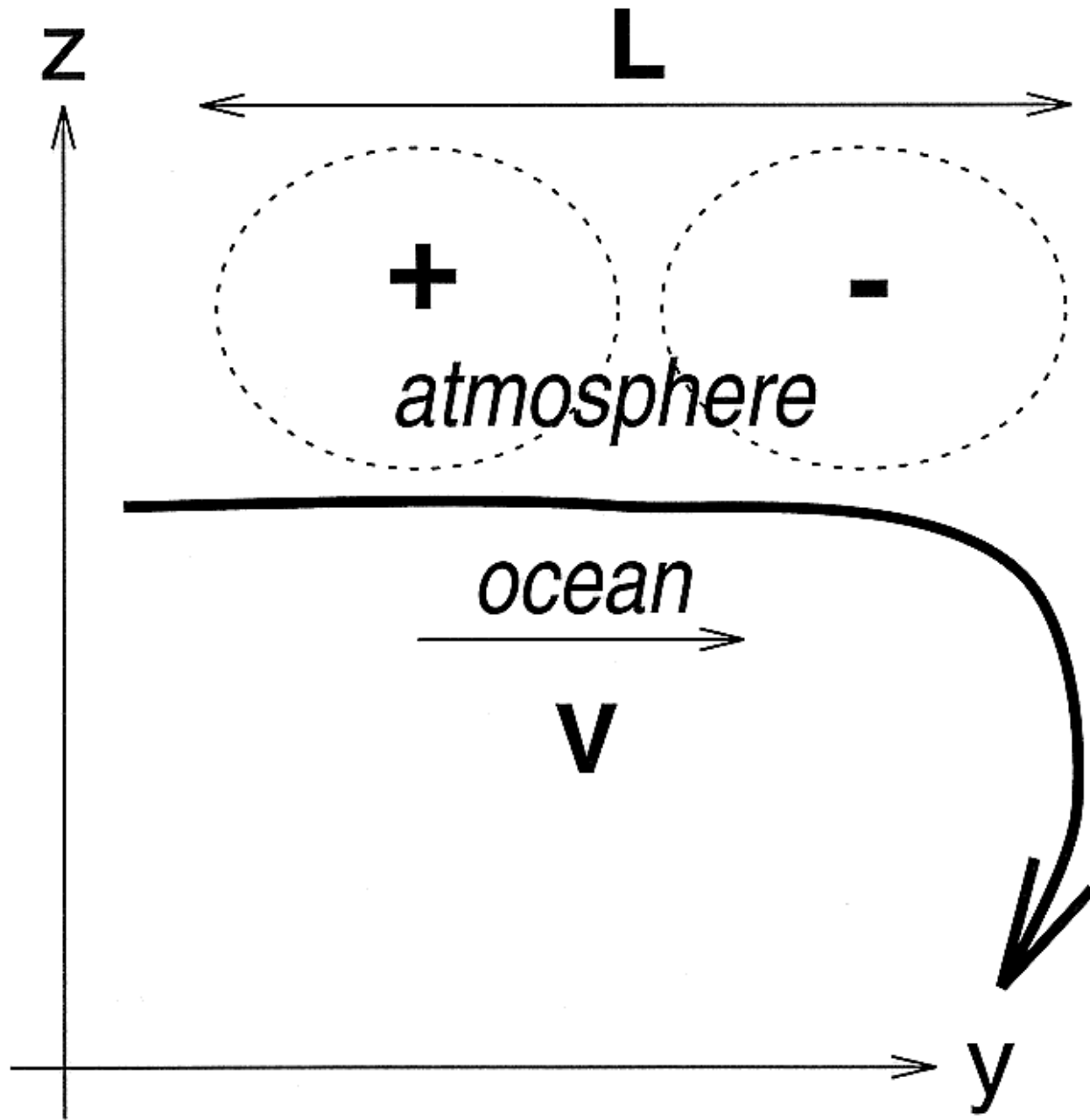
Stochastically forced spatial resonance

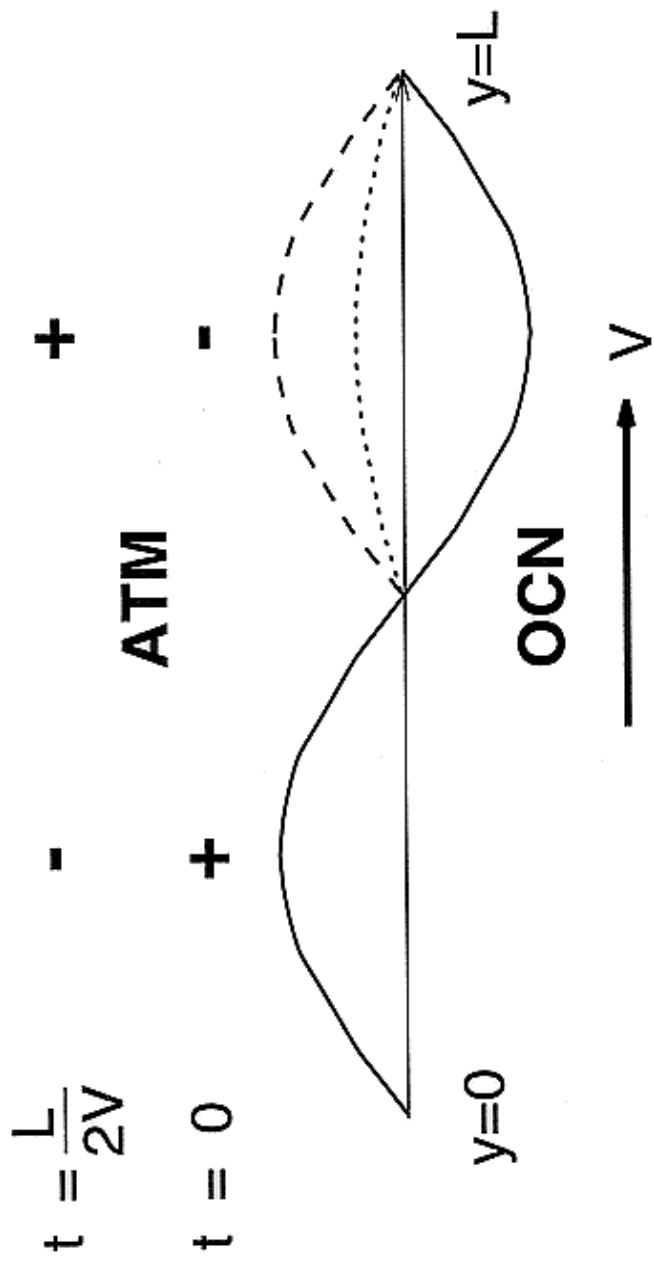


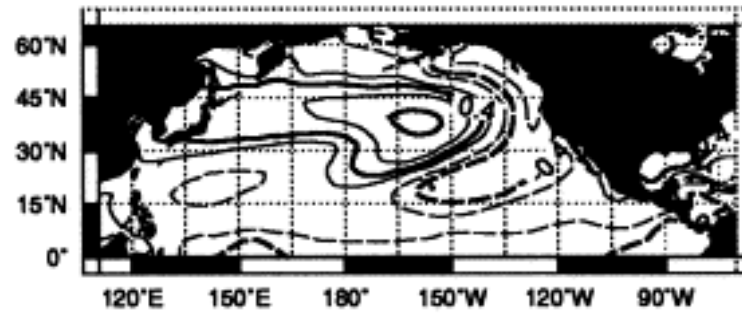
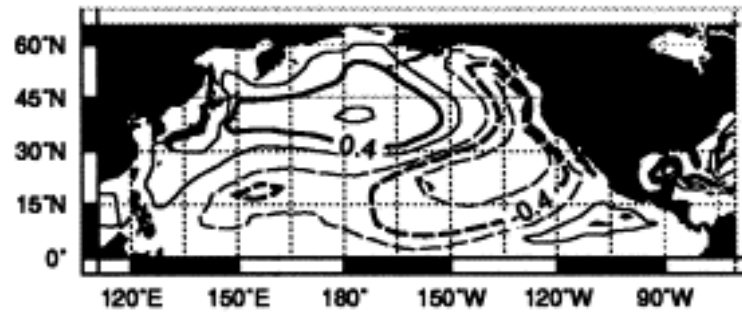
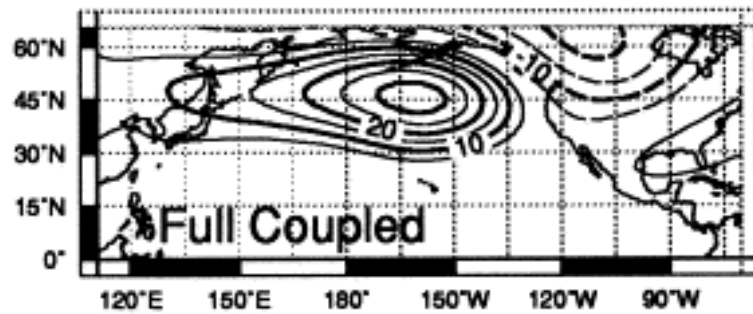
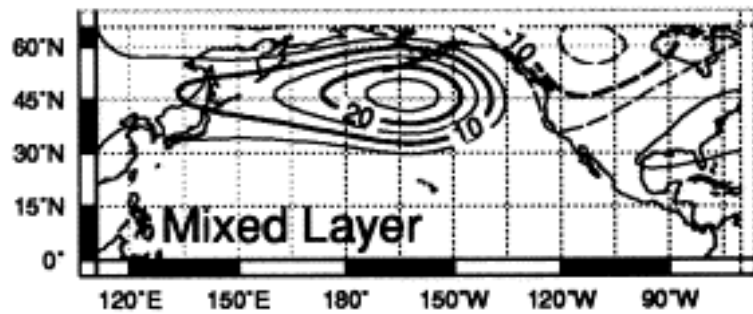
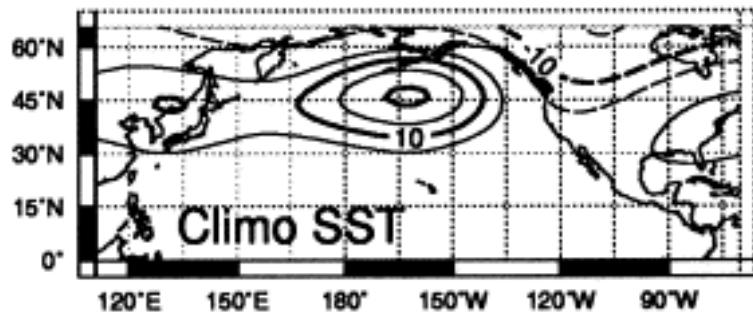
Response of ocean to stochastic forcing only



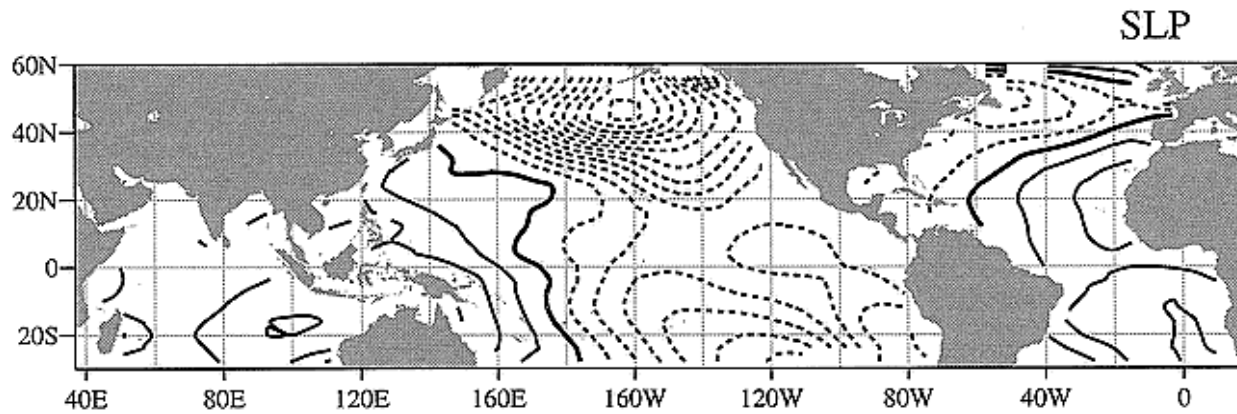
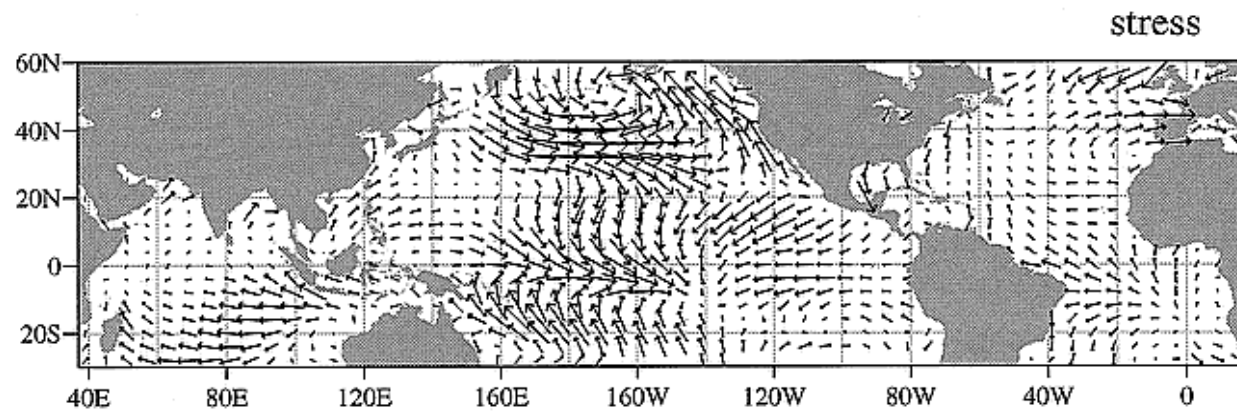
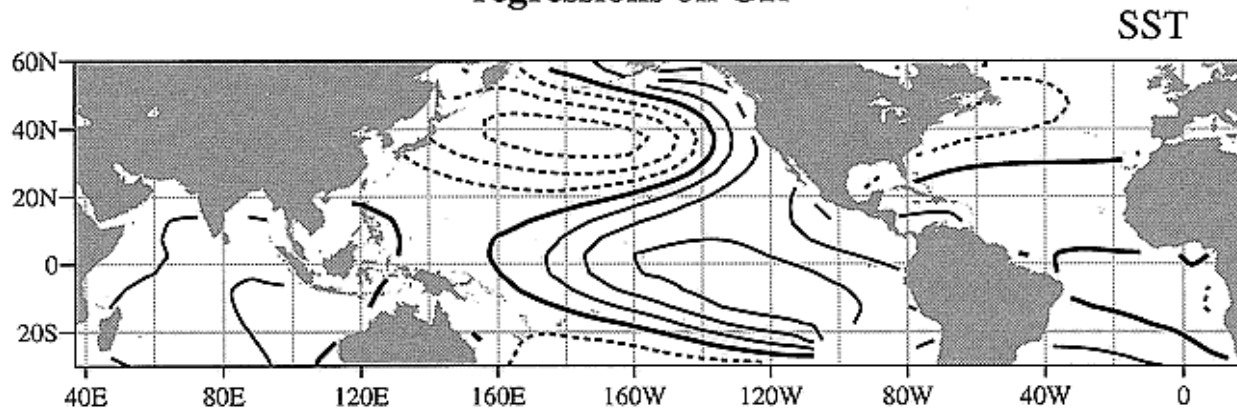
PAU





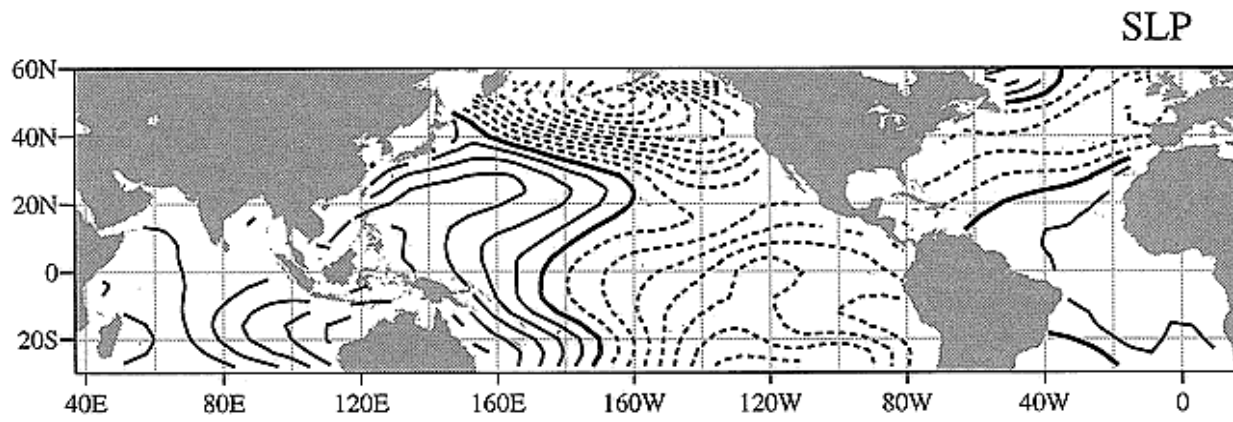
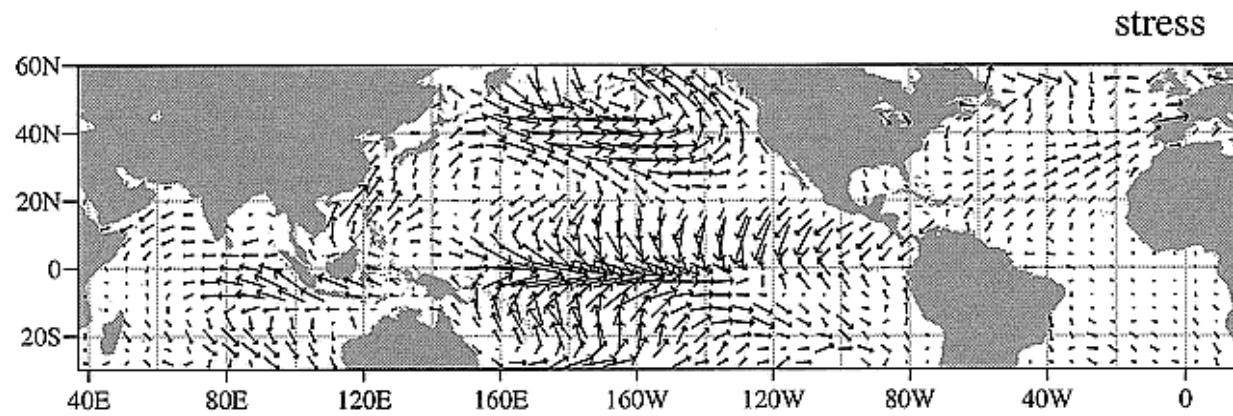
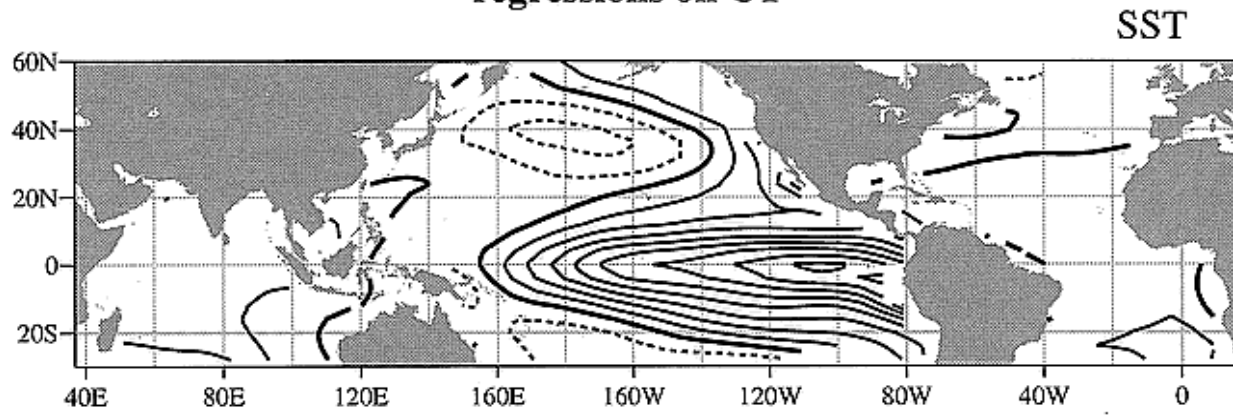


regressions on GR



Zhang, Wallace, Battisti 1997

regressions on CT*



Zhang, Wallace, Battisti 1997

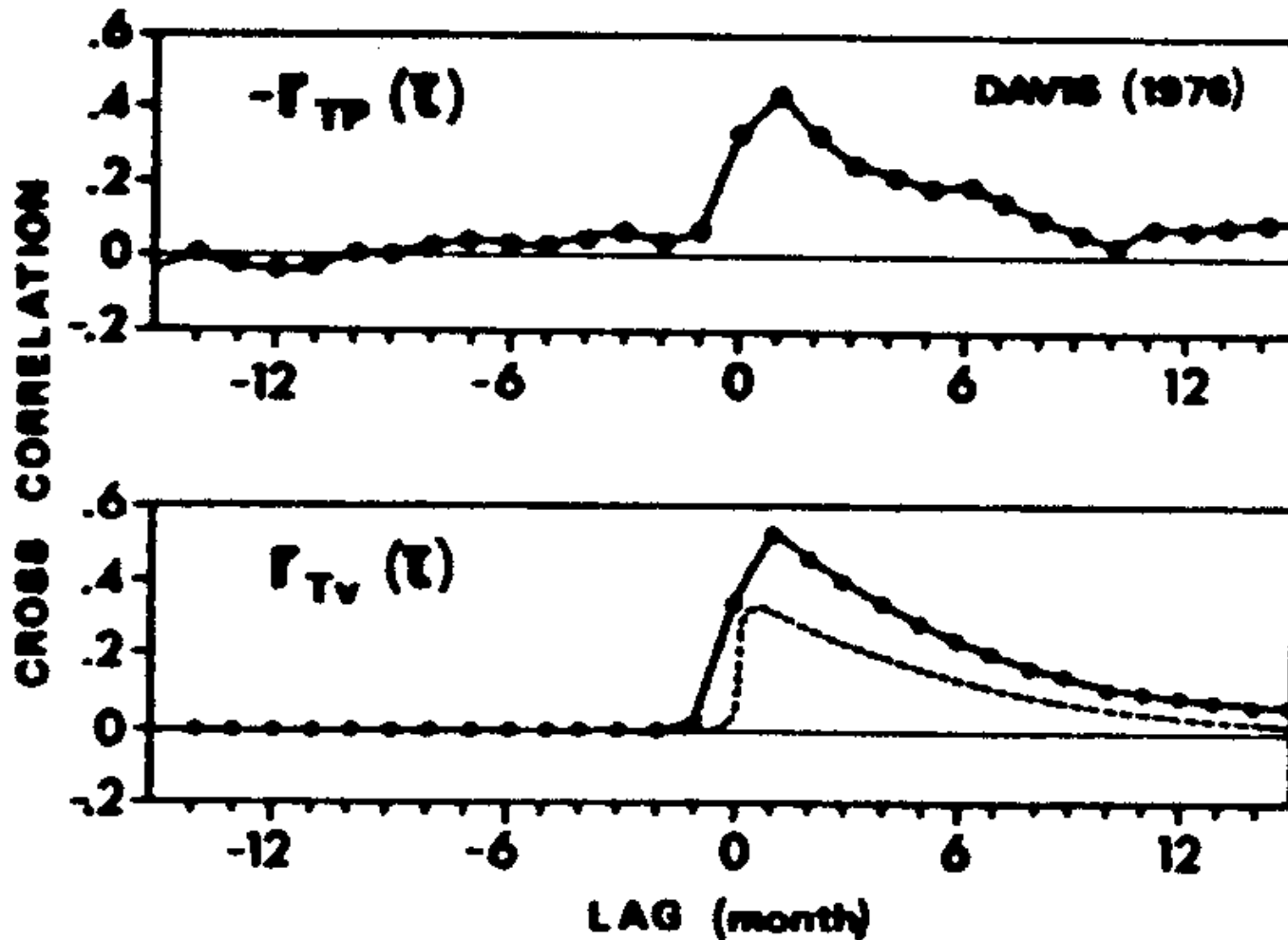


Fig. 20. (Top) Observed correlation between the dominant empirical orthogonal function of SST and sea level pressure anomalies over the North Pacific as estimated by *Davis* [1976]. (Bottom) Theoretical correlation for $\nu = (8.5 \text{ day})^{-1}$, $\lambda = (6 \text{ month})^{-1}$ without smoothing (dashed line) and as estimated from monthly averaged data (continuous line).